DESIGN AND ANALYSIS IN MODELLING REACTIVE SEPARATION PROCESSES

By

Gerardo J. Ruiz Mercado

A Thesis submitted in partial fulfillment of the requirements for the degree of

DOCTOR OF PHILOSOPHY
in
CHEMICAL ENGINEERING

UNIVERSITY OF PUERTO RICO
MAYAGÜEZ CAMPUS
2008

Approved by:

_____	_____
Lakshmi Sridhar, PhD President, Graduate Committee	Date
_____	_____
Jaime Benítez, PhD Member, Graduate committee	Date
_____	_____
Gilberto Villafañe, PhD Member, Graduate committee	Date
_____	_____
Lorenzo Saliceti, PhD Member, Graduate committee	Date
_____	_____
Lynette Orellana, PhD Representative of Graduate Studies	Date
_____	_____
David Suleiman, PhD Chairperson of the Department	Date

Abstract

This work presents the existence of multiple steady states in equilibrium multistage reactive distillation for methyl tert-butyl ether (MTBE) synthesis. The Rachford-Rice procedure is extended to reactive systems where a continuation analysis was applied using the Damköhler number for an isothermal reactive flash process involving both MTBE and tertiary amyl methyl ether (TAME) mixtures exhibiting Hopf bifurcations. The Extension of this analysis to non-equilibrium models shows the existence of limit points in the case of the TAME mixture and isolas with intersecting branches in the case of the MTBE mixture. New expressions to calculate the nonequilibrium residue composition maps for reactive separation processes incorporating mass transfer effects and design aspects were derived. For MTBE synthesis it was demonstrated that reactive saddle-point azeotrope calculated by equilibrium and non-equilibrium approaches are not the same and for TAME synthesis the nonequilibrium and equilibrium reactive composition curve maps in the limit of reaction equilibrium were obtained.

Resumen

En este trabajo investigativo se muestra la existencia de Múltiples Estados Estacionarios en el modelamiento de una columna de destilación reactiva en equilibrio de fases para la síntesis de metil terbutil éter (MTBE). El procedimiento de Rachford-Rice se extiende a sistemas de separación con reacción tipo flash, luego a este esquema se le aplica un análisis de continuación utilizando el número de Damköhler, y se estudia la producción de MTBE y teramil metil éter (TAME) donde en ambos sistemas se encontraron bifurcaciones tipo Hopf. El análisis anterior fue extendido a un sistema unitario de separación reactiva de no-equilibrio donde se muestra la existencia de bifurcaciones tipo límite en la síntesis de TAME y el fenómeno de curvas cerradas tipo “isolas” junto con ramificaciones interceptadas en la producción de MTBE. Se derivó una nueva expresión para calcular los mapas residuales de composición donde se incorporó el efecto de transferencia de masa junto a configuraciones de diseño. Con la síntesis de MTBE se demostró que los modelos de equilibrio y no-equilibrio no coinciden en la localización de azeótropos reactivos, y se reportó un mapa de curvas de composición en el límite de la reacción para la producción de TAME.

Acknowledgments

I would like to thank God to stay with me every time, to my wife Carola Barrera, my daughters Itzel and Eluney Ruiz Barrera, my parents Gerardo Ruiz and Ana Mercado, my sisters Ana and Yenis Ruiz Mercado, and my parents in law Idelilliam Cuadro and Samuel Barrera, for their unconditional support, inspiration, and love. I would also like to express my gratitude to the people who helped me through my graduate studies at the University of Puerto Rico at Mayaguez, especially my advisor Professor Lakshmi Sridhar. Thanks to Professor Jaime Benitez for his academic and humanistic wisdom, he is like my father in Puerto Rico. I am grateful for the financial support of the NSF (grant number CTS 0341608), the Chemical Engineering Department, and AGEP Puerto Rico.

Contents

List of Tables

List of Figures

Publication that resulted from this work:

- Design of Non-Equilibrium Reactive Separation Processes. Gerardo Ruiz and L. N. Sridhar. Submitted to *Industrial Engineering & Chemistry Research*. 2008.

- Singularities in Reactive Separation Processes. Gerardo Ruiz, M. Diaz and L. N. Sridhar, *Industrial Engineering & Chemistry Research*. 2008, 47, 2808-2816.

- The Isothermal Isobaric Reactive Flash Problem. Gerardo Ruiz, L. N. Sridhar and R. Rengaswamy, *Industrial Engineering & Chemistry Research*. 2006, 45, 6548-6554.

Chapter 1 Introduction

There has been an on growing interest in the design and optimization of reactive distillation systems because they offer an alternative procedure to conventional processes. Reactive distillation (RD) combines the key operations of most chemical processes into one unit: chemical reaction and distillation. RD has several applications to processes as methyl tert-butyl ether (MTBE) production, synthesis of tertiary amyl methyl ether (TAME), metathesis of alkenes, etc.

The typical RD equipment is comprised of a non hybrid scheme where reaction and separation occur simultaneously in all stages, and a hybrid system where the column is divided into three regions, one for reactions and separation and two for separation only. Like conventional distillation columns the RD towers are made by using trays or packing[1], and can be used to carry out both homogeneous and heterogeneous catalyzed chemical reactions[2-4].

Mathematical models of several complexities for RD have been commonly applied in MTBE and TAME synthesis. All models can be enclosed in two: the equilibrium reactive model (EQ) which adopts an equilibrium stage approach with a reaction rate expression, and the more complex non-equilibrium (NEQ) model that takes into account both finite reaction rates and finite interface mass and energy transfer fluxes. Multiple steady states (MSS) behavior has been reported previously involving both EQ and NEQ models, but a detailed analysis of

reactive distillation process that involve the identification of the singular point that cause theses multiplicities is necessary.

During reactive separations, complex interactions between reaction kinetics and mass transfer operations occurs introducing strong nonlinearities. The interactions between vapor-liquid mass and energy transfer and chemical kinetics increase the complexity of modeling and scale up of RD processes. Therefore, a study of the effect(s) of mass transfer on the multiplicity regions will have significant implications in column design, operation, and control.

Residue curve maps play an important role in the design of reactive separation processes. Barbosa and Doherty[5] and Ung and Doherty[6] have derived a set of differential equations to model the reactive simple distillation with multiple reactions expressed in terms of transformed composition variables using the equilibrium model. Castillo and Towler[7], Taylor et al.[8], and Sridhar et al.[9, 10] addressed departures from equilibrium to draw composition trajectories to locate azeotropes in non-reactive systems. They showed that the azeotrope calculated with EQ and NEQ models coincide. But, what effect does the mass transfer have on the distillation lines and in the location of the NEQ reactive azeotrope? Will the NEQ and EQ reactive azeotropes coincide as in the non-reactive case?

This work presents the existence of multiple steady states in multistage reactive distillation, singular points and MSS in NEQ and EQ single stage reactive separation processes, and finally the non-equilibrium reactive composition curve maps are calculated showing that stationary reactive points calculated by equilibrium and non-equilibrium models are not the same.

1.1 Objectives

The objectives of this work are:

- To investigate the causes for the multiplicity that occurs in equilibrium and non-equilibrium reactive distillation processes
- To locate the singularities that cause these MSS
- To design and construct tools to investigate the effect of kinetics and mass transfer on feasible splits for NEQ reactive separation processes.

Chapter 2 Modelling and Simulation of Equilibrium Reactive Distillation Columns

The equilibrium reactive model is applied to study the metathesis of 2-pentene and MTBE synthesis using the algorithm implemented by Chen et al.[11] to find the steady state solution. Simultaneously two methods to solve nonlinear algebraic equation system are applied where multiple steady states are found for MTBE process.

2.1 Introduction

Figure 2-1(a) shows a schematic diagram of the equilibrium stage. In the equilibrium reactive model the vapor and liquid leaving the stage are assumed to be in equilibrium with each other. A complete reactive separation process is modeled as a series of *j* equilibrium stages (Figure 2-1(b)). The general model is comprised of partial and total material balance equations, energy balance for each stage, and the phase equilibrium relation.

The equations that describe the equilibrium stages are:

The material balance for each component and the total material balance,

$$\frac{d\left(\varepsilon_j x_{ij}\right)}{dt} = F_j z_{ij} + L_{j-1} x_{i\,j-1} + V_{j+1} y_{i\,j+1} - V_j y_{ij} - L_j x_{ij} + \varepsilon_j \sum_{m=1}^{r} v_{m,i} R_{j,m} \tag{2.1}$$

$$\frac{d\varepsilon_j}{dt} = F_j + L_{j-1} + V_{j+1} - V_j - L_j + \varepsilon_j \sum_{m=1}^{r} v_{m,T} R_{j,m} \tag{2.2}$$

Where x_{ij} and y_{ij} are the liquid and vapor molar fractions respectively for the component *i* in the stage *j*, ε_j is the total holdup for stage *j*, $R_{j,m}$ is the reaction rate for *m* reaction in the stage

j, and $\nu_{m,i}$ is the stoichiometric coefficient i in reaction m, $\nu_{m,T} = \sum_{i=1}^{c} \nu_{m,i}$, c is the total number of components in the mixture, F_j is the total feed to stage j, z_{ij} is the molar feed composition for the component i in the stage j, L_j is the liquid molar flow leaving from stage j, and V_j is the vapor molar flow leaving from stage j. The stages are numbered from the top to bottom as shown in Figure 2-1(b).

The following relation is used to account for the phase equilibrium,

$$y_{i,j} = K_{i,j} x_{i,j} \tag{2.3}$$

where K_{ij} is the phase equilibrium constant for the component i in the stage j.

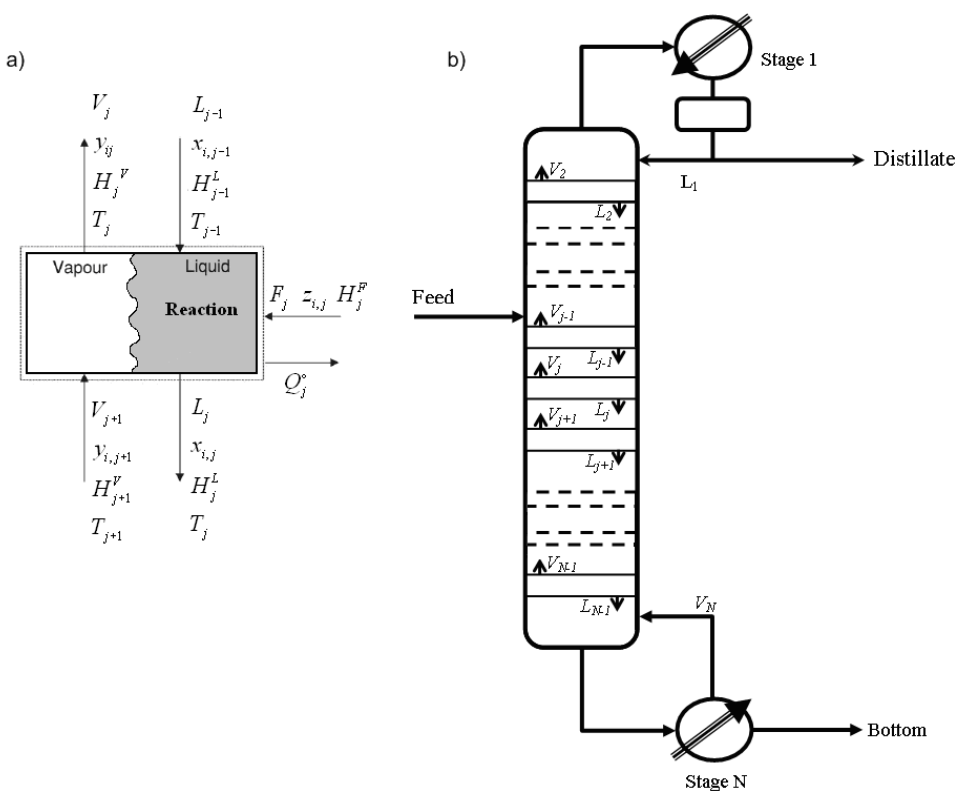

Figure 2-1. a) Equilibrium stage. b) Equilibrium multistage column.

The summation of liquid and vapor mole fraction is given by,

$$\sum_{i=1}^{c} x_{i,j} = 1 \tag{2.4}$$

$$\sum_{i=1}^{c} y_{i,j} = 1 \tag{2.5}$$

Finally, the enthalpy balance is defined as,

$$\frac{d\left(\varepsilon_j H_j\right)}{dt} = F_j H_j^F + L_{j-1} H_{j-1}^L + V_{j+1} H_{j+1}^V - V_j H_j^V - L_j H_j^L + Q^{\circ}{}_j \tag{2.6}$$

where H_j is the molar enthalpy of the stage j, H_j^L and H_j^V are the liquid and vapor enthalpy respectively for the stage j, and $Q^{\circ}{}_j$ heat flow transferred to or from the surroundings for the stage j.

2.2 Multistage Reactive Distillation Column

The system of nonlinear simultaneous differential and algebraic equations was solved at steady state by three different methods: the Chen et al.[11] algorithm, the trust region dogleg method, and the Levenberg-Marquardt method[12]. The Chen et al.[11] algorithm solved the nonlinear algebraic equation dynamically using a small integrating time, whereas the last two methods are algorithms to solve directly nonlinear algebraic equation systems that have different predictor steps and convergence criteria. The model was validated for efficiency and robustness using the metathesis of 2-pentene process.

2.2.1 Model Equations

Rearranging and adjusting equation (2.1) based on Chen et al.[11] assumption (constant total molar holdup) gives

$$\frac{d\left(x_{ij}\right)}{d\tau}=\frac{\varepsilon_T}{F_T}\frac{1}{\varepsilon_j}\left(F_j z_{ij}+L_{j-1}x_{i\,j-1}+V_{j+1}y_{i\,j+1}-V_j y_{ij}-L_j x_{ij}\right)+\frac{\varepsilon_T}{\varepsilon_T^R}\frac{\mathrm{Da}}{k_{f,\mathrm{ref}}}\delta_j\sum_{r=1}^{R}\left(v_{r,i}R_{j,r}\right) \tag{2.7}$$

Where $F_T=\sum_{j=1}^{N}F_j$ is the total feed flow to column, $\varepsilon_T=\sum_{j=1}^{N}\varepsilon_j$ is the total molar holdup of the column, $d\tau=\left(F_T/\varepsilon_T\right)dt$, and $\varepsilon_T^R=\sum_{j=1}^{N}\left(\delta_j\varepsilon_j\right)$ is the molar holdup summation when reaction occurs in stage j and $\delta_j=1$, for all others $\delta_j=0$.

The Damköhler number is a dimensionless ratio of a characteristic liquid residence time $\left(\varepsilon_T^R/F\right)$ and the characteristic reaction time $\left(1/k_{f,\mathrm{ref}}\right)$, $\mathrm{Da}=\left(\varepsilon_T^R/F\right)/\left(1/k_{f,\mathrm{ref}}\right)$. $k_{f,\mathrm{ref}}$ is the forward reaction rate at a temperature of reference. This dimensional number allows to study simultaneously the reaction and physical separation phenomena using Da>>1 when the reaction equilibrium limit is reached and Da<<1 when only non-reactive separation is achieved.

The Da number plays an important role in this work; it is used as a continuation parameter to investigate the multiplicity behavior at steady state condition $\left(d\left(x_{ij}\right)/d\tau=0\right)$.

2.3 Metathesis of 2-pentene

This is an ideal process for reactive distillation applications.

The equimolar reversible reaction of 2-pentene to form 2-butene and 3-hexene is shown in the equation below:

$$2C_5H_{10} \Leftrightarrow C_4H_8 + C_6H_{12} \tag{2.8}$$

Equation (2.7) is solved at steady state assuming the same configuration system as in Chen et al.[11] and using Da=7 to match the design model assumption made by Okasinski and Doherty[13]

as exposed in Table 2-1. Figure 2-2 shows the comparison between the Chen et al.[11] simulation and the experimental results of Okasinski and Doherty[13]. As can be seen, the simulation and design results are in good agreement. Our temperature and liquid compositions profiles shown in Figure 2-3 are identical to the profiles obtained by Chen et al.[11] (Figure 2-4).

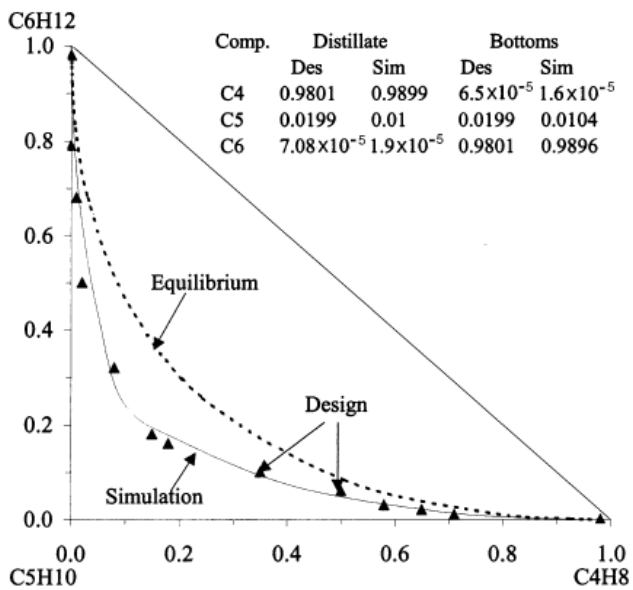

Figure 2-2. Metathesis of 2-pentene. Comparison between Chen et al. (2000) simulation results (solid line) and design results (filled triangles) of Okasinski and Doherty (1998) Da=7.

Table 2-1. Specifications for the simulation of the metathesis system

Number of stages	14
Feed location	7
Feed quality	1
Feed rate	100 kmol/h
Feed composition [x_{C4H8}, x_{C5H10}, x_{C6H12}]	[0.0, 1.0, 0.0]
Reflux ratio	4.0
Reboil ratio	5.0

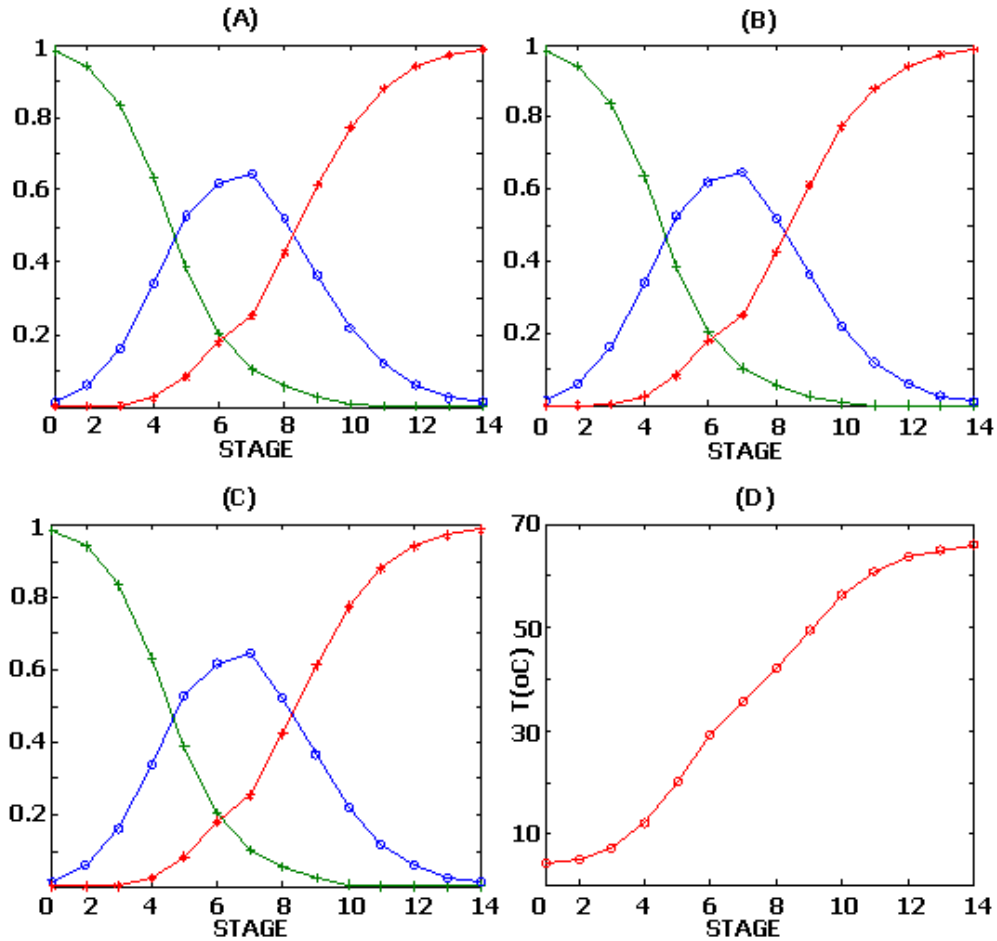

Figure 2-3. Steady state liquid compositions profile for metathesis of 2-pentene found by three different methods. Solution by: (A) Chen et al. (2000) algorithm, (B) trust region Dogleg method, and (C) Levenberg-Marquardt method. Green(+): x_{C4H8}, Blue(o): x_{C5H10}, Red(*): x_{C6H12}. (D) Steady state temperature profile.

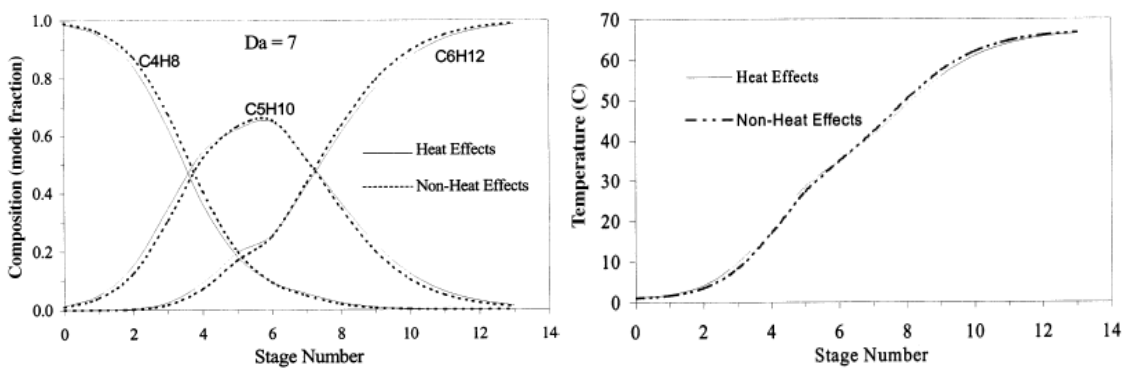

Figure 2-4. Steady state liquid compositions and temperature profiles for metathesis of 2-pentene by Chen et al. (2000).

2.4 Multiple Steady States in Reactive Distillation

MSS in conventional distillation have been known from simulation and theoretical analysis[14-16]. Figure 2-5 shows the MSS phenomenon for MTBE production, where each line represents a steady state profile of the MTBE molar fraction in the vapor phase through the column stages. On the first rigorous analysis of non-equilibrium separation processes, provided by Sridhar et al.[10, 17], the MSS occurred in the phase equilibrium calculations at the interface. Pisarenko et al.[18] first reported a MSS in RD where they found three steady states for a RD column, two of which were stable. MSS in RD have been also demonstrated by other several workers[1, 4, 11, 19-24] where the most commonly investigated situation involves the MTBE synthesis in the Jacobs and Krishna[25] column configuration. In this case two steady states were found originated from two different paths that correspond to two different kinds of residual curves.

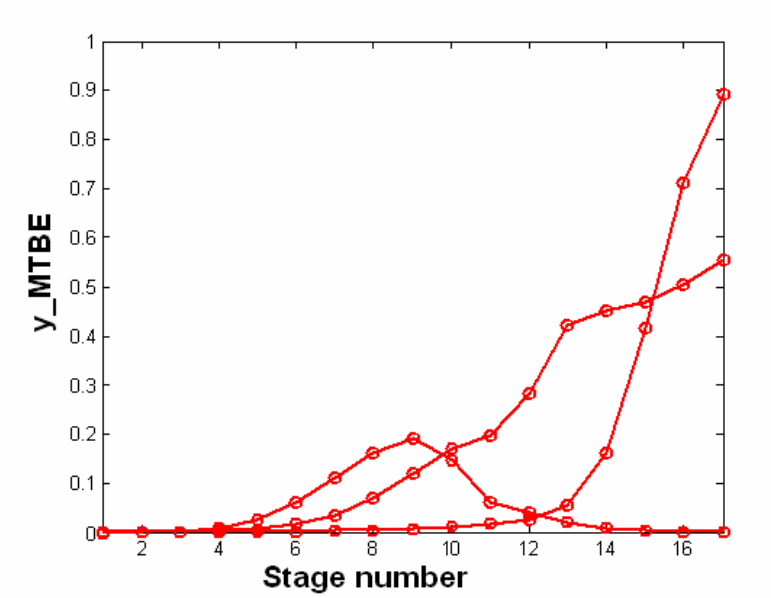

Figure 2-5. MSS for MTBE production, vapor MTBE composition.

Another situation is the TAME synthesis in the column configuration of Mohl et al.[26]. They showed that multiple steady states for the TAME process are originated by kinetic instabilities.

Recently experimental and simulation studies of the MSS existences have been performed by Mueller and Marquardt[27] for non reactive system. Rapmund et al.[28] performed experiments for the TAME production where multiplicities were observed as function of the start-up procedure utilized. Mohl et. al.[26] revealed that only theoretical and experimental studies at the same time enable the possibility to verify experimentally the existence of MSS.

2.5 MTBE Production

The MTBE (CH_3COCH_3) is produced by liquid phase esterification reaction from methanol (MeOH) and *i*-butene. This reaction is highly selective, and only occurs in the presence of other olefins[29], which operates as an inert component, such as n-butane:

$$i\text{-butene}+\text{MeOH}+\text{n-butane} \rightleftharpoons \text{MTBE}+\text{n-butane} \tag{2.9}$$

In this simulation, the configuration used is described in the Figure 2-6 with Da = 100. The thermodynamic equilibrium constant, the reaction rate constant, and the rate equation were taken from Venimadhavan et al.[30].

The rate model that describes the kinetics of MTBE synthesis catalyzed by H_2SO_4 is:

$$R = 4464 * \exp\left(-3187 / T\left(K\right)\right)\left[\left(a_{i\text{-butene}}\right)\left(a_{\text{MeOH}}\right) - \frac{a_{\text{MTBE}}}{8.33E-8 * \exp(6820 / T\left(K\right))}\right] \tag{2.10}$$

where T is the temperature in Kelvin, and a is the activity. The boiling point temperature of isobutene at 11 atm (328.15 K) is chosen as the reference temperature to calculate $k_{f,\text{ref}} = 0.4882\,\text{h}^{-1}$. The non ideality of the liquid phase is represented by the Wilson equation using the thermodynamic data taken from Table 3.3 in Barbosa[31] and Table 3 in Ung and Doherty[32].

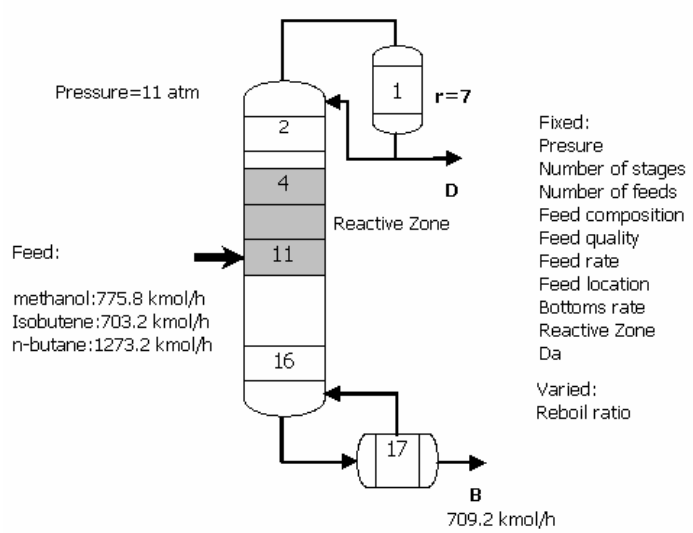

Figure 2-6. Column configuration and feed specifications for MTBE system.

Three steady states were found at low, intermediate, and high isobutene conversion. The plots for the liquid compositions and temperature profile for high conversion at steady state are shown in Figure 2-7.

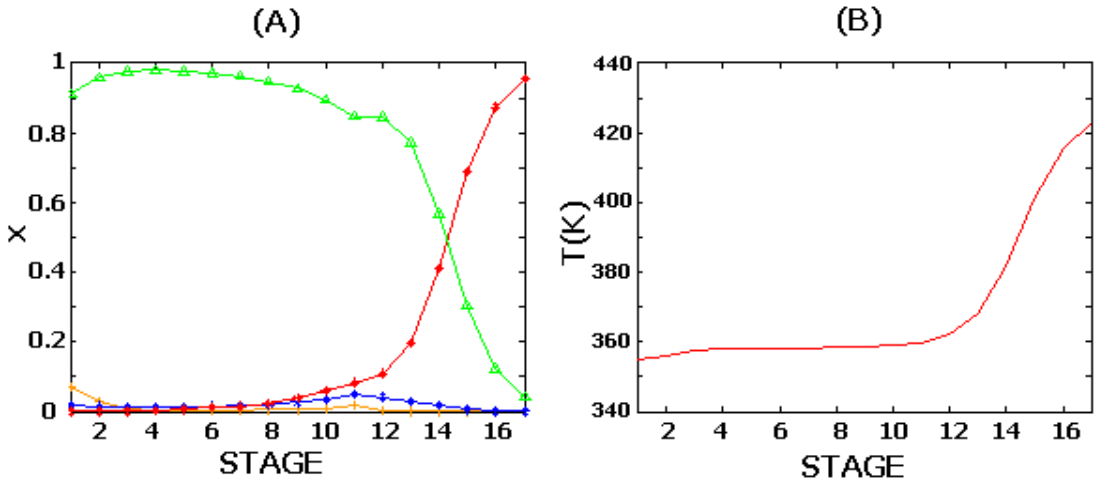

Figure 2-7. A) High conversion MTBE steady state liquid compositions profile. Orange (+): $x_{methanol}$, blue(o): $x_{i\text{-}butene}$, red(*): x_{MTBE}, green(Δ): $x_{n\text{-}butane}$. B) Steady state temperature profile.

At a Damköhler number of 100 the system produces multiple solutions but at low *Da* (~<*50*) this phenomenon does not occur. The appearance of either state depends on the initial state of

the column (initial liquid compositions and temperature profiles). A possible phenomenon responsible for the multiple steady states can be the non ideality of the liquid mixture. Another explanation is a combination of physical separation and the presence of an exothermic chemical equilibrium reaction inside the column.

Plots for the temperature and liquid composition profiles for intermediate and low conversion steady state are illustrated in Figure 2-8 and Figure 2-9 respectively, showing the effect when the forward equilibrium reaction is displaced to the products (left side of the reaction) and the decrease of the MTBE composition in the last stages (rectifying zone).

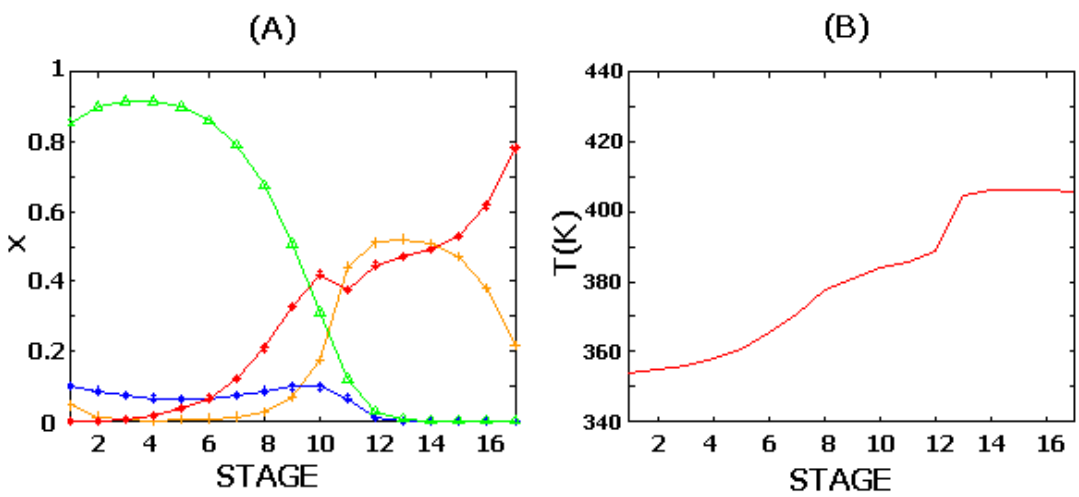

Figure 2-8. A) Intermediate conversion MTBE SS liquid composition profiles. B) Steady state temperature profile.

2.6 Conclusions

A steady state analysis of the equilibrium reactive distillation problem using the Damköhler number was performed. The metathesis of 2-pentene was used to validate the accuracy of the strategy employed then extended to the MTBE production to show MSS phenomenon. The Da

number is an important parameter in modeling reactive distillation processes because it produces multiplicities at critical values.

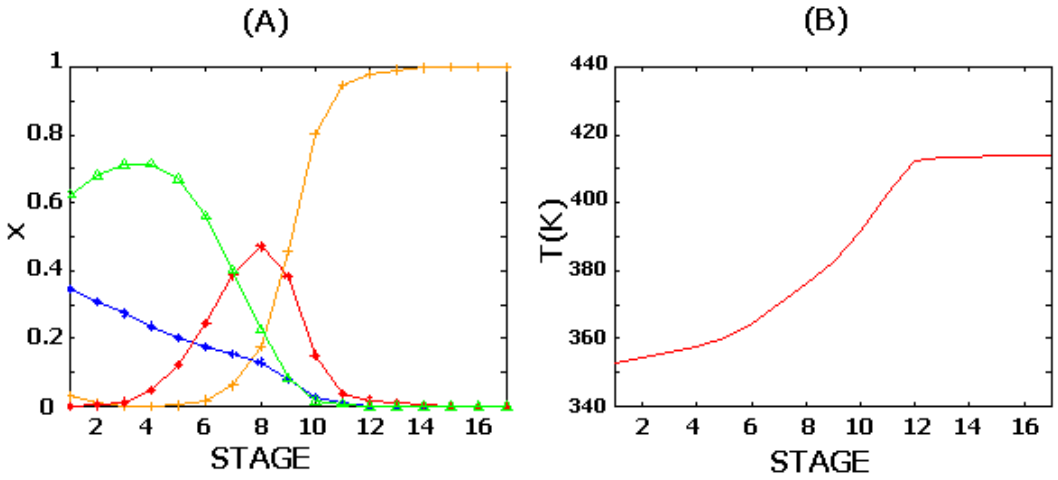

Figure 2-9. A) Low conversion MTBE SS liquid composition profiles. B) Steady state temperature profile.

Chapter 3 Equilibrium Continuation

The continuation method is applied to solve ordinary differential equations (ODE) and systems of differential algebraic equations (DAE) at steady state conditions. It computes a successive sequence of points of solutions which are function of an active parameter (i.e. Da). The continuation method localizes singular points which produce multiple solutions. We use throughout this work a numerical continuation program called CL_MATCONT.

3.1 Numerical Continuation[33]

A numerical continuation is a technique that computes a consecutive sequence of point's solution which approximates the desired branch[33]. Most continuation algorithms implement a prediction of a new point and correction of the predicted point. This method produces a succession of points x_i, $i = 1, 2, ...$ along the curve fulfilling a chosen convergence criterion.

As an illustration, consider a differential equation

$$\frac{du}{dt} = f(u, \alpha) \tag{3.1}$$

where $u \in \mathbf{R}^n$, $\alpha \in \mathbf{R}$, and $f : \mathbf{R}^{n+1} \rightarrow \mathbf{R}^n$

At steady state, $f(u, \alpha) = 0$, and defining a new function $F(x)$,

$$F(x) = f(u, \alpha) = 0 \tag{3.2}$$

Suppose we have found a point x_i on the curve, with $x = (u, \alpha) \in \mathbf{R}^{n+1}$ and defining a normalized tangent vector v to the equilibrium curve at x as $v \in \mathbf{R}^{n+1}$. In this case, $F_x(x) \cdot v = 0$

and $\langle v, v \rangle = 1$. The computation of the next point x_{i+1} consists of two steps: the prediction of a new point, and the correction of the predicted point.

3.1.1 Prediction

Step size h is an important parameter in the continuation algorithm since too small step-sizes can lead to additional unnecessary numerical work, while too big step-sizes may lead to lose details of the solution curve. A frequently used predictor is the tangent prediction:

$$X^0 = x_i + h v_i \tag{3.3}$$

3.1.2 Correction

It is assume that X^0 is close to the solution curve. To find the next point x_{i+1} on the curve we use a modified Newton procedure. Since the standard Newton iterations can only be applied to square systems (# equations= # unknowns), an extra scalar condition is added:

$$\begin{aligned} F(x) &= 0 \\ g(x) &= 0 \end{aligned} \tag{3.4}$$

The function $g(x)$ could be a hyperplane passing through X^0 that is orthogonal to the vector v_i:

$$g(x) = \langle x - X^0, v_i \rangle \tag{3.5}$$

then, the Newton iteration turns into:

$$X^{k+1} = X^k + H_x^{-1}(X^k) H(X^k) \tag{3.6}$$

where $H(X) = \begin{pmatrix} F(X) \\ 0 \end{pmatrix}$ and $H_x(X) = \begin{pmatrix} F_x(X) \\ v_i^T \end{pmatrix}$

when the point x_{i+1} is found, we have to calculate the tangent vector in this point:

$$\begin{pmatrix} F_x(x_{i+1}) \\ v_i^T \end{pmatrix} v_{i+1} = \begin{pmatrix} 0 \\ 1 \end{pmatrix} \tag{3.7}$$

3.2 CL_MATCONT

We use the program CL_MATCONT[33] for drawing the continuation diagram and locating the singular points in the next chapters. The prediction-correction continuation algorithm used here is based on the Moore-Penrose pseudo-inverse matrix to obtain the solution curve for the equation set $F(x)=0$ for a function $F:\mathbf{R}^{n+1}\to\mathbf{R}^{n}$. The Moore-Penrose pseudo-inverse matrix for a $N\times(N+1)$ matrix A is defined as

$$A^{+}=A^{T}(AA^{T})^{-1} \tag{3.8}$$

To obtain $A^{+}b$, where $b\in\mathbf{R}^{N}$, a system is made for which $x\in\mathbf{R}^{N+1}$ such that

$$\begin{aligned} Ax&=b\\ v^{T}x&=0\\ Av&=0 \end{aligned} \tag{3.9}$$

where $x=A^{+}b$ is a solution to this system.

For a curve $F(x)=0$ where $F:\mathbf{R}^{n+1}\to\mathbf{R}^{n}$ a tangent vector v^{i} should satisfy

$$F_{x}(x^{(i)})v^{(i)}=0 \tag{3.10}$$

For a point $x^{(i)}$ on the curve, the prediction of the next point is tangential and this will lead to the Moore-Penrose correction (see Dhooge et al.[33] for details)

$$X^{k+1}=X^{k}-F_{x}^{+}(X^{k})F(X^{k}) \tag{3.11}$$

For the computation of $F_{x}^{+}(X^{k})$ CL_MATCONT uses the approximation

$$F_{x}^{+}(X^{k-1})V^{k}=0 \tag{3.12}$$

Once all these functions are defined the correction procedure in CL_MATCONT is simple as described by Dhooge et al. (2004).

$$A=F_{x}(X^{k}) \tag{3.13}$$

$$B = \begin{pmatrix} A \\ V^{k^T} \end{pmatrix} \tag{3.14}$$

$$R = \begin{bmatrix} AV^k \\ 0 \end{bmatrix} \tag{3.15}$$

$$Q = \begin{bmatrix} F(X^k) \\ 0 \end{bmatrix} \tag{3.16}$$

The correction procedure would yield

$$W = V^k - B^{-1}R \quad V^{k+1} = \frac{W}{\| W \|} \tag{3.17}$$

$$X^{k+1} = X^k - B^{-1}Q \tag{3.18}$$

This iteration procedure is repeated until a certain tolerance is attained.

3.3 Bifurcations[33, 34]

The bifurcations produce multiplicity (paths) in the solution of a continuous system that depends on the active parameter (i.e. α, Da). With the solution evaluated at each active parameter value is possible to make a branching diagram as shown in the Figure 3-1. The bifurcation can be detected along the steady state equilibrium curve.

In continuous systems there are several types of bifurcations[34]. For this work only three types of bifurcation will be considerate because they have physical significance in reactive separation processes.

- Fold bifurcation: also known as limit point, denoted by LP (Figure 3-1), this type of singular point frequently arises in pairs, showing hysteresis effects. In situations a LP separates stable from unstable behavior and indicate that two solutions are born or two solutions extinguish each other.

- Hopf bifurcation: denoted as H (Figure 3-2), is the type of bifurcation that connects a SS branch (equilibrium) with periodic state (a branch of periodic oscillations). At H point there is an exchange of stability from stable equilibrium to stable limit cycle that encircles the unstable equilibrium
- Branching bifurcation: denoted by BP (Figure 3-1), is a point where two branches intersect. A BP where various braches intersect is called multiple BP, and it can produce an isola curve.

Three test functions are defined to detect these singularities[33]:

$$\phi_1(u,\alpha) = \det\begin{pmatrix} F_x \\ v^T \end{pmatrix} \tag{3.19}$$

$$\phi_2(u,\alpha) = \det\left(2\, f_u(u,\alpha) \odot I_n\right) \tag{3.20}$$

$$\phi_3(u,\alpha) = v_{n+1} \tag{3.21}$$

where $\odot$ is the bialternate matrix product or byproduct. For example If $f_u(u,\alpha)$ is an $n \times n$ matrix and I_n is the $n \times n$ identity matrix, then the byproduct $2\, f_u(u,\alpha) \odot I_n$ is an $m \times m$ matrix where $m = n(n-1)/2$. If the matrix components are pairs (i, j) with $i > j$, the bialternate matrix product is defined by[35]:

$$\left(2\, f_u(u,\alpha) \odot I_n\right)_{(i,j),(k,l)} = \begin{cases} -a_{il} & \text{if } k = j \\ a_{ik} & \text{if } k \neq i \text{ and } l = j \\ a_{ii} + a_{jj} & \text{if } k = i \text{ and } l = j \\ a_{jl} & \text{if } k = i \text{ and } l \neq j \\ -a_{jk} & \text{if } l = i \\ 0 & \text{otherwise} \end{cases} \tag{3.22}$$

.

The singularities can be defined using these test function:

BP: $\phi_1 = 0$

H: $\phi_2 = 0$

LP: $\phi_3 = 0$ and $\phi_1 \neq 0$

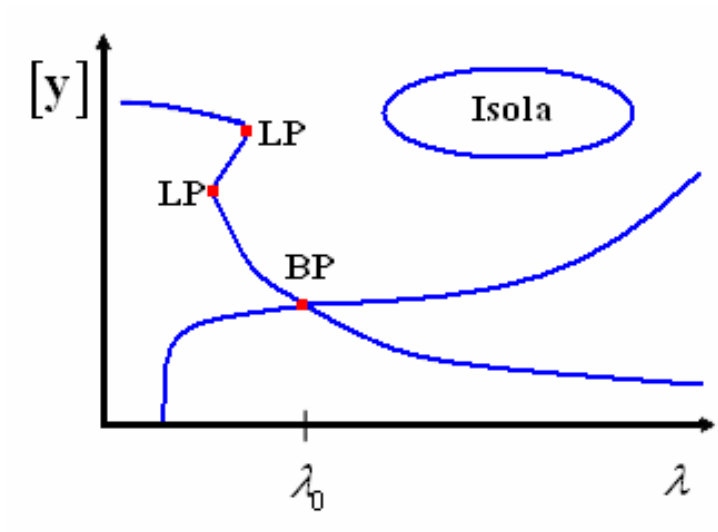

Figure 3-1. A fictive branching diagram

3.3.1 Branching Point Locator[33]

The location of LP and H points normally does not cause inconvenient, but the location of BP can give problems. This difficulty can be avoided by using $p \in \mathbf{R}^n$ and $\beta \in \mathbf{R}$ and considering the extended system:

$$\begin{aligned} f(u,\alpha) + \beta p &= 0 \\ f_u^T(u,\alpha)p &= 0 \\ p^T f_\alpha(u,\alpha) &= 0 \\ p^T p - 1 &= 0 \end{aligned} \tag{3.23}$$

This system is solved by the Newton's method with initial values β=0 and $p : f_u^T p = \mu p$ where μ is the closed to zero real eigenvalue. A BP (u,α) corresponds to a regular solution $(u,\alpha,0,p)$.

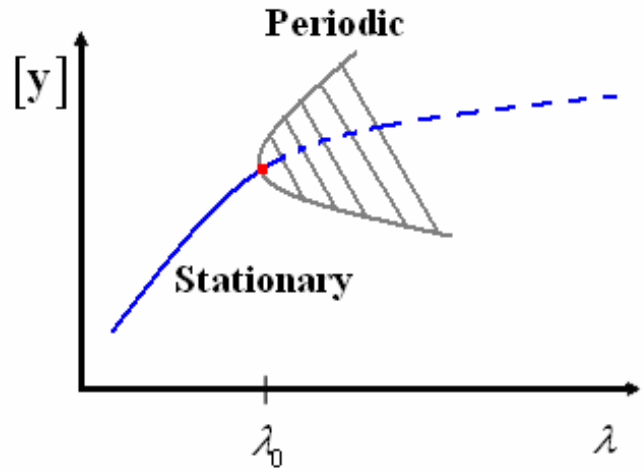

Figure 3-2. Hopf bifurcation illustrated in branching diagrams.

Chapter 4 The Equilibrium Single Stage Reactive Separation Problem

In this chapter we present some results for the isothermal isobaric reactive separation process. We show that the Rachford-Rice procedure can be extended to reactive systems. We also demonstrate that even in isothermal isobaric reactive separation processes which is probably the least nonlinear of all reactive separation processes we get nonlinear phenomena such as Hopf bifurcations. While it has been shown that Hopf bifurcations are impossible in isothermal CSTR problems and also in non-reactive flash problems, we demonstrate in this chapter that isothermal reactive flash processes involving both MTBE and TAME mixtures exhibit Hopf bifurcations.

4.1 Introduction

During the last decade there has been a tremendous interest in the field of reactive distillation. A review of the various models used in reactive distillation can be found in Taylor and Krishna[36]. Of special interest is the existence of multiple steady-states in these problems, since the combination of separation and reaction can in principle introduce the nonlinearity that can cause multiplicity. Multiple steady-states in reactive distillations was demonstrated by several workers[1, 4, 19, 22-26, 28, 37-42]. The most commonly investigated situations include the MTBE synthesis in the Jacobs-Krishna[25] column configuration and the TAME Synthesis in the column of Mohl et al.[26]. The multiple steady-states for these two columns were investigated by Chen

et. al.[4] who concluded that multiplicities are lost for high values of Da for TAME, while the opposite is found for MTBE. This conclusion, however is specific to the column configuration described in Jacobs-Krishna[25] and Mohl et. al.[26]. Rodriguez et. al. [43, 44] discussed causes for the existence of multiple steady-states in binary and ternary systems. Unfortunately, the most important reactive separation process problems where multiplicity exists such as MTBE and TAME processes involve more than three components. In order to understand what causes multiplicity in these problems one must look at the simplest reactive separation process problem involving the MTBE and TAME mixture such as the isothermal reactive flash problem. Mohl et. al.[26] prove that isothermal CSTR problems do not exhibit Hopf bifurcations while, on the other hand, for non-reactive isothermal flash processes involving homogeneous mixtures Hopf bifurcations are impossible[45]. However we demonstrate that isothermal reactive flash processes involving both TAME and MTBE exhibit Hopf bifurcations. In this chapter a brief description of the isothermal reactive flash process is first given along with the equations involved. A modified Rachford-Rice[46] procedure for solving the isothermal reactive separation process problem is presented. We then demonstrate the existence of Hopf bifurcations in the isothermal reactive flash processes involving both the MTBE and TAME mixtures. Dynamic simulations are performed demonstrating the existence of limit cycles that are a characteristic feature of problems with Hopf bifurcations and the behavior of these singular points with temperature and pressure variations are presented.

4.2 The Isothermal Reactive Separation Flash Problem

For a single stage reactive separation unit with a single reaction, equation (2.7) is set as,

$$\frac{dx_i}{d\tau} = \frac{1}{F}\left(Fz_i - Vy_i - Lx_i\right) + \frac{\mathrm{Da}}{k_{f,\mathrm{ref}}}\left(v_i R\right) \tag{4.1}$$

At steady state and using $\frac{\mathrm{Da}}{k_{f,\mathrm{ref}}} = \frac{\varepsilon}{F}$ equation (2.6) is reduced to:

$$\frac{1}{F}\left(Fz_i - Vy_i - Lx_i\right) + \frac{\varepsilon}{F}\left(v_i R\right) = 0 \tag{4.2}$$

where F is the external feed, L is the liquid flow, V the vapor flow, ε the holdup, R the extent of reaction and ν the stoichiometric coefficient.

We also have the phase equilibrium equation (2.3) for a single stage

$$y_i = K_i x_i \tag{4.3}$$

Where the physical equilibrium constant is defined as:

$$K_i = \frac{\gamma_i P_i^{\mathrm{sat}}}{P} \tag{4.4}$$

And the summation expression for both phases (equation (2.4) and (2.5))

$$\sum_{i=1}^{c} y_i = 1 \tag{4.5}$$

$$\sum_{i=1}^{c} x_i = 1 \tag{4.6}$$

The total number of equations and variables are equal to $2c + 2$ which includes equations (4.2), (4.3), (4.5), and (4.6) and variables x_i, y_i, L, and V respectively. This set of equations at steady state can be solved by specifying T, P, and ε. While this set of equations at steady state can be solved using a variety of techniques, a modified Rachford-Rice procedure for solving the isothermal isobaric reactive flash problem is presented in the next section.

4.3 Modified Rachford -Rice Procedure

We solve the set of equations (4.2), (4.3), (4.5), and (4.6) using a modified Rachford Rice procedure.

Defining $\varepsilon\left(\nu_i R\right) = \Re_i$ and $\dfrac{\left(\sum_{i=1}^{c} \Re_i\right)}{F} = \Xi$, we obtain from equation (4.2),

$$z_i - \frac{V}{F} y_i - \frac{L}{F} x_i + \frac{\Re_i}{F} = 0 \tag{4.7}$$

Substituting equation (4.3) and re-arranging we get

$$z_i + \frac{\Re_i}{F} = \left(\frac{L}{F} + \frac{V}{F} K_i\right) x_i \tag{4.8}$$

or

$$x_i = \frac{z_i + \dfrac{\Re_i}{F}}{\left(\dfrac{L}{F} + \dfrac{V}{F} K_i\right)} \tag{4.9}$$

and

$$y_i = K_i \left(\frac{z_i + \dfrac{\Re_i}{F}}{\dfrac{L}{F} + \dfrac{V}{F} K_i} \right) \tag{4.10}$$

Since $\sum_{i=1}^{c} (y_i - x_i) = 0$ we have

$$\sum_{i=1}^{c} \left(\frac{z_i + \dfrac{\Re_i}{F}}{\dfrac{L}{F} + \dfrac{V}{F} K_i} \right) \left(K_i - 1\right) = 0 \tag{4.11}$$

If $\dfrac{V}{F} = \alpha$, $\dfrac{L}{F} = 1 - \Xi - \alpha$ we get

$$\sum_{i=1}^{c}\left(\frac{z_i+\frac{\Re_i}{F}}{(1-\Xi-\alpha)+(\alpha)K_i}\right)(K_i-1)=\Phi(\alpha)=0 \tag{4.12}$$

The derivative of this function with respect to α will be

$$-\sum_{i=1}^{c}\left(\frac{z_i+\frac{\Re_i}{F}}{\left((1-\Xi-\alpha)+(\alpha)K_i\right)^2}\right)(K_i-1)^2=\Phi'(\alpha) \tag{4.13}$$

Using the method of Newton we can compute α in the inner loop and obtain both $\frac{V}{F}=\alpha$ and $\frac{L}{F}=1-\Xi-\alpha$. The liquid and vapor compositions can be corrected in the outer loop using equations (4.9) and (4.10) .

4.4 TAME Process

Tertiary amyl methyl ether (TAME) is generated from methanol and a mixture of isoamylenes 2-methyl-1-butene (2MB1) and 2-methyl-2-butene (2MB2) reacting in liquid phase using a sulphonic acid ion exchange resin as catalyst[47-49] and n-pentane as inert. Three reactions take place simultaneously,

Reaction 1: $$\text{2MB1+MeOH} \rightleftharpoons \text{TAME} \tag{4.14}$$

Reaction 2: $$\text{2MB2+MeOH} \rightleftharpoons \text{TAME} \tag{4.15}$$

Reaction 3: $$\text{2MB1} \rightleftharpoons \text{2MB2} \tag{4.16}$$

Only two of the above three reactions are independent. Adding equations (4.14) and (4.15),

Reaction 4: $$(2.0)\text{MeOH}+2\text{MB1}+2\text{MB2} \rightleftharpoons (2.0)\text{TAME} \tag{4.17}$$

Since the isomerisation (reaction 3) is very fast in comparison to the TAME reactions[47] the rate model for reaction 4 is

$$R_4 = k_{f4}\left(\frac{a_{\text{2M1B}}}{a_{\text{MeOH}}} - \frac{1}{K_1}\frac{a_{\text{TAME}}}{a_{\text{MeOH}}^2}\right) \tag{4.18}$$

And for a catalyst activity of 1.2 (eq H^+)/(kg catalyst)[26]:

$$k_{f4} = \left(1+K_3\right)\left(1.9769\text{x}10^{10}\right)\exp\left(-\frac{10764}{T}\right) \tag{4.19}$$

The equilibrium constants[50]

$$K_1 = 1.057\text{x}10^{-4}\,\text{e}^{4273.5/T} \tag{4.20}$$

and

$$K_3 = 0.648\text{e}^{899.9/T} \tag{4.21}$$

4.5 Solution Procedure

At steady state equation (4.1) can be re-written as

$$\left(z_i - \theta_V y_i - \theta_L x_i\right) + \frac{\text{Da}}{k_{f,\text{ref}}}\left(v_i R\right) = 0 \tag{4.22}$$

where $\theta_L = L/F$ and $\theta_V = V/F$ and $k_{f,\text{ref}}$ is the forward rate constant evaluated at the boiling point of the lowest boiling pure component in the system. This temperature value is 328.15 K for the MTBE process and 334.15 K for the TAME process. Using the Damköhler number as the continuation parameter we solve equations (4.22), (4.3), (4.5) and equation (4.6) using the program CL_MATCONT[33]. Details of the algorithm and the strategy for the numerical

equilibrium continuation and obtaining the location of the bifurcation points are presented in Chapter 3 and Dhooge et al.[33].

4.6 Hopf Bifurcations in a MTBE TP Reactive Separation Flash

In this section we demonstrate the existence of Hopf bifurcations in an isothermal isobaric (TP) reactive separation flash problem. Consider a reactive separation TP flash for the MTBE synthesis problem. In this problem, isobutene reacts with methanol to produce MTBE using n-butane as an inert component. The rate model and the activity coefficient parameters are given in Section 2.5 using components ordered as [isobutene, methanol, MTBE and n-butane]. For a feed composition of [0.163 0.005 0.081 0.751], a pressure of 11 atm, and a temperature of 363.22 K[51] the program CL_MATCONT (Chapter 3) was used to draw the continuation curve by using the Damköhler number as the continuation parameter. Two Hopf bifurcation points were found at the Damköhler values of 1.495 and 5.128 as shown in Figure 4-1. We performed a dynamic simulation for two different starting points were for each of the Hopf points a periodic oscillation and a convergence to a steady-state were obtained characteristic of a Hopf bifurcation point. The periodic oscillation and the convergence to the steady-state at the first Hopf point are shown in Figure 4-2 and Figure 4-3 respectively. similar results were found for the second Hopf bifurcation point. Figure 4-4 shows the Hopf points at various temperatures were it can be observed that at a temperature of 363.25 K and beyond one of the Hopf points disappears. A similar behavior is observed when the total pressure of the system is changed as shown in Figure 4-5 where it is seen that as the pressure is lowered below 11 atmospheres one of the Hopf points disappears.

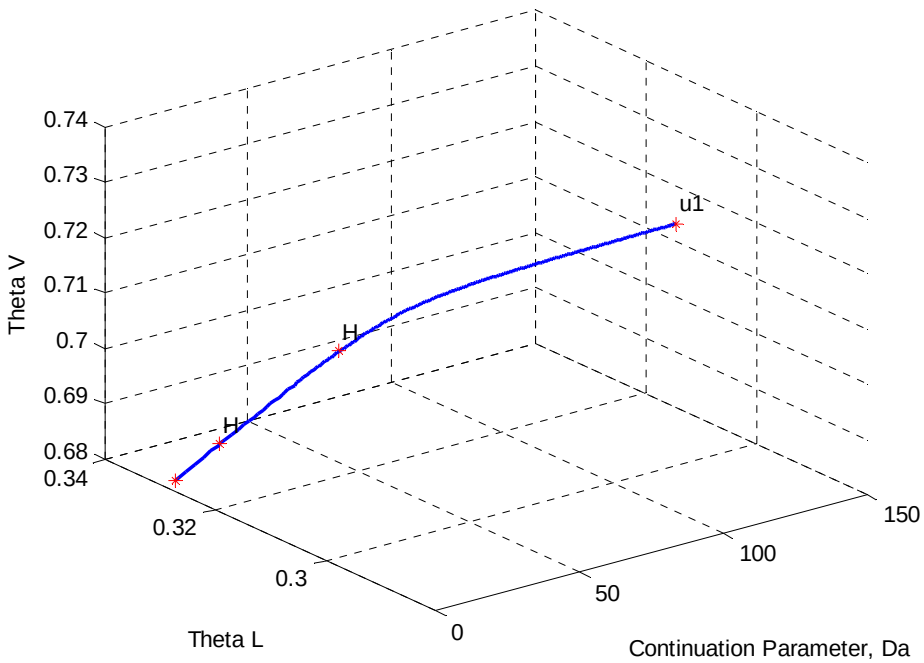

Figure 4-1. Continuation diagram for MTBE synthesis.

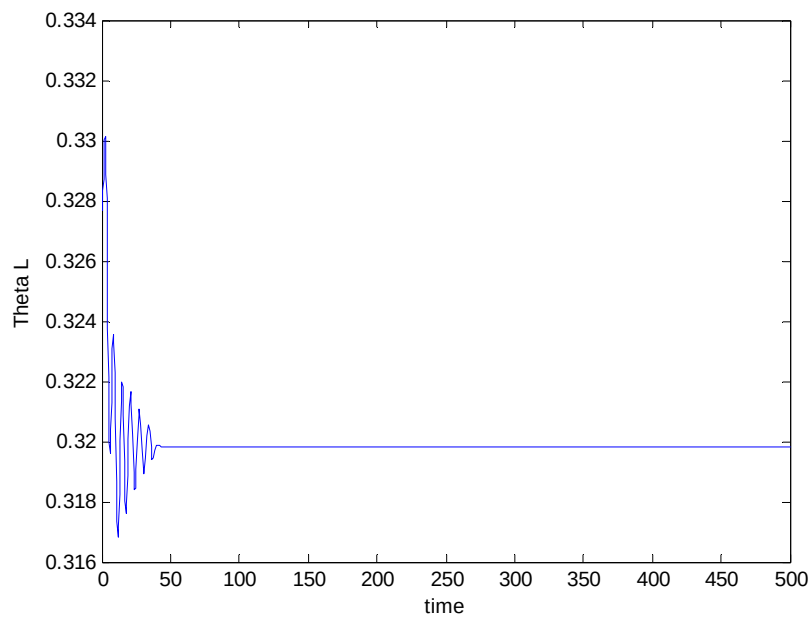

Figure 4-2. Hopf point 1. Convergence to steady state.

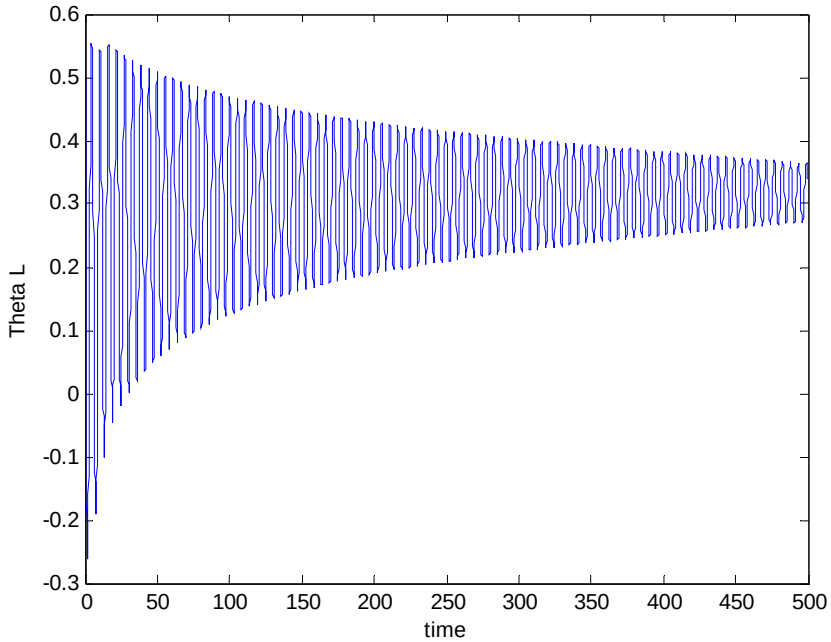

Figure 4-3. Hopf point 1. Periodic oscillation.

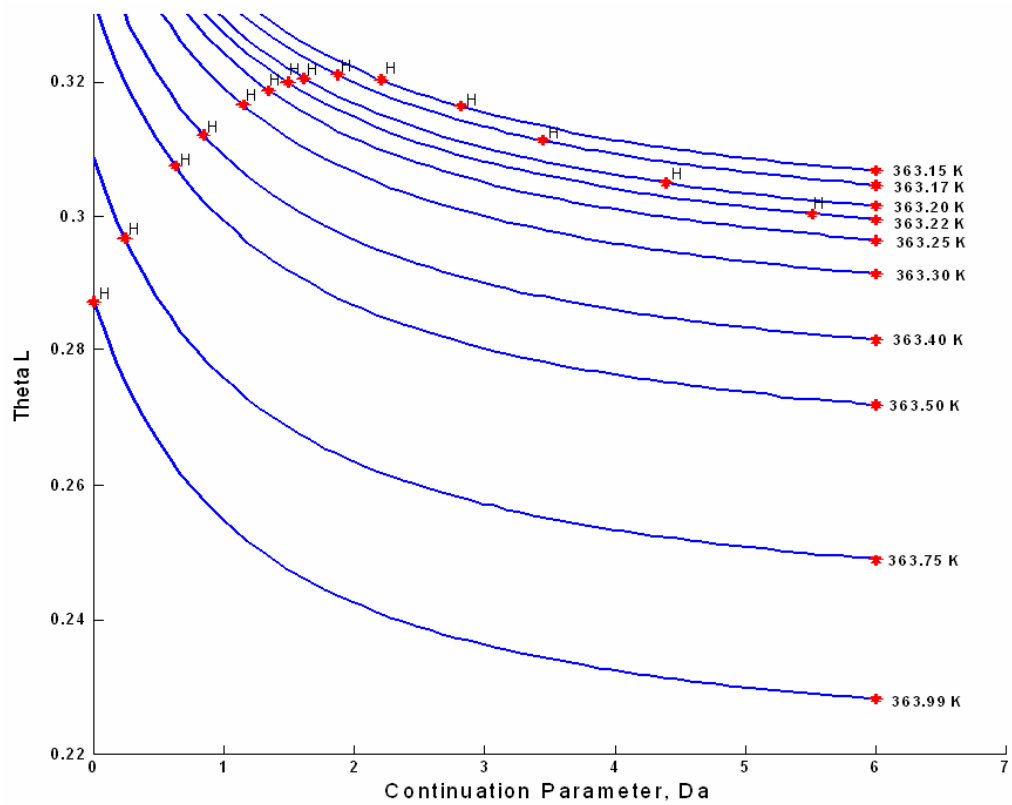

Figure 4-4. Hopf bifurcation points at various temperatures

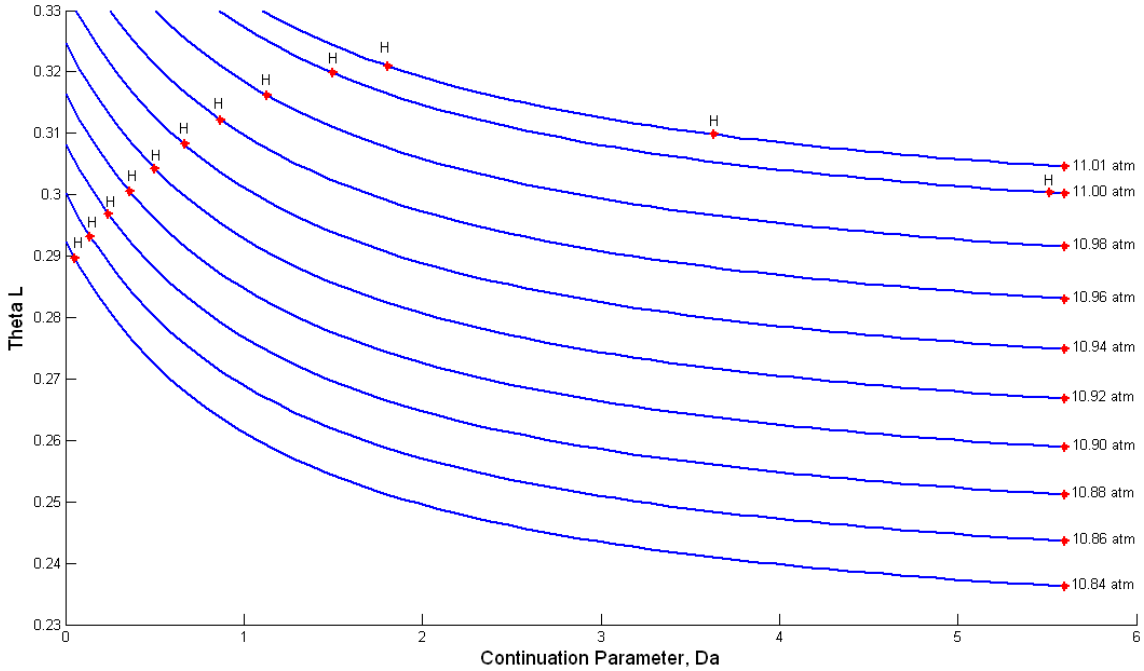

Figure 4-5. Hopf bifurcation points at different Pressures.

4.7 Hopf Bifurcations in an Isothermal Isobaric TAME Process

Performing a similar analysis as in section 4.6 now for TAME synthesis, a Hopf bifurcation point at a Damköhler number of 0.4620 was obtained at 335K and 2.55 atmospheres as shown in Figure 4-6 using components ordered as MeOH, 2M1B, 2M2B, TAME and n-pentane at a feed composition of [0.2647; 0.0463; 0.2846; 0; 0.4044]. Figure 4-7 and Figure 4-8 show the existence of a limit cycle and a steady-state at this Damköhler value. Figure 4-9 shows the existence of the Hopf bifurcation point at various temperatures while Figure 4-10 shows the Hopf bifurcation points at various pressures. These results clearly demonstrate the existence of Hopf bifurcations in isothermal reactive flash processes. It is possible that under certain operating conditions these Hopf bifurcations can exist in multistage columns too and such columns may need special control mechanisms like delayed feedback control.

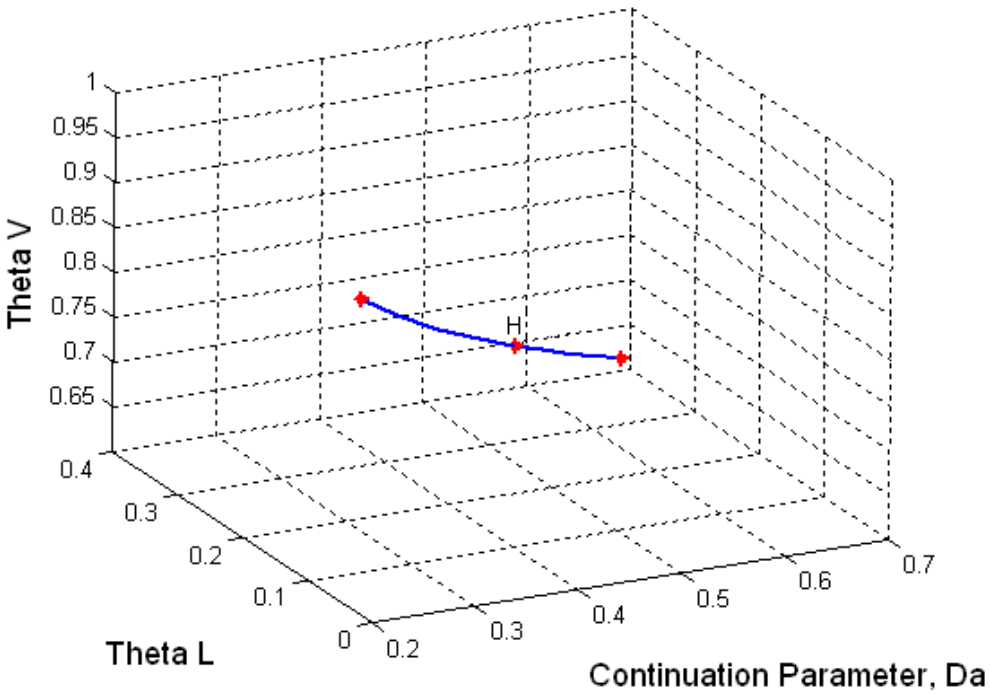

Figure 4-6. Continuation diagram for TAME problem

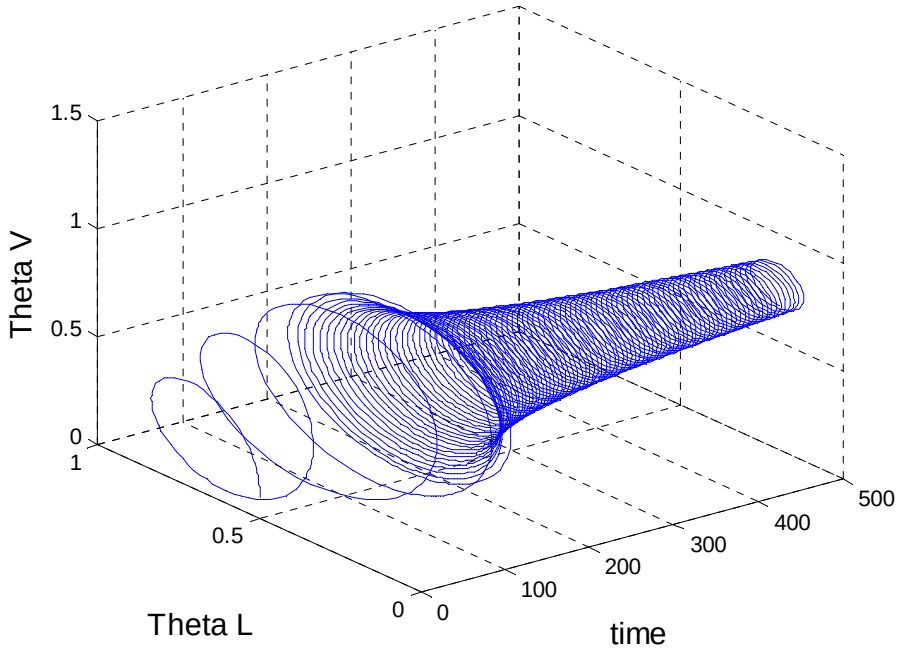

Figure 4-7. Hopf point, periodic oscillations for TAME problem.

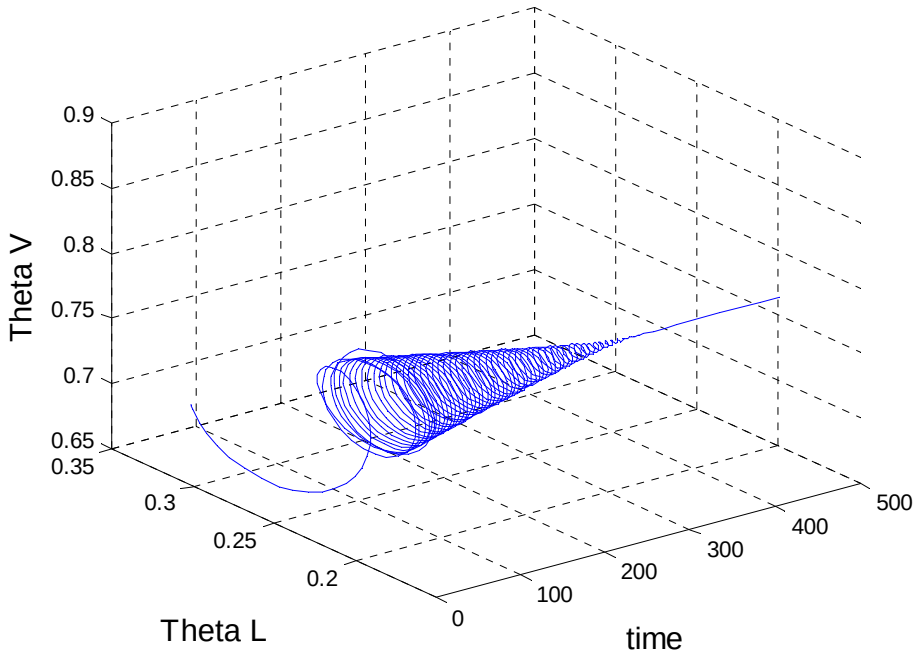

Figure 4-8. Hopf point, convergence to steady state.

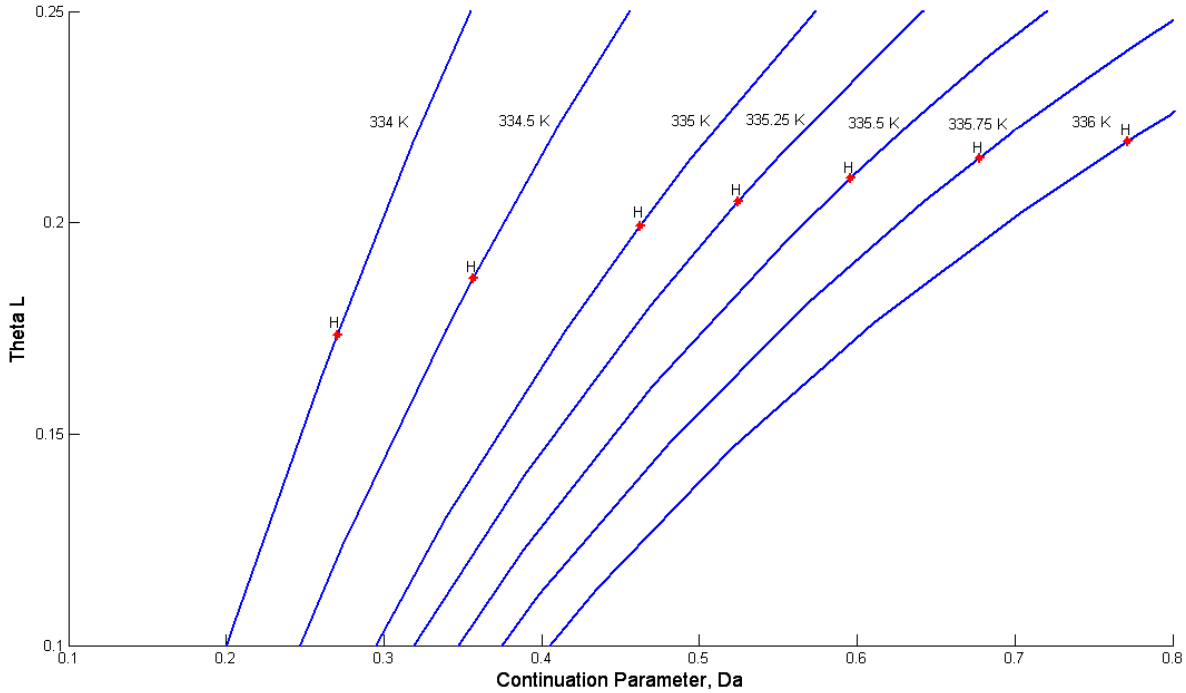

Figure 4-9. The behavior of the Hopf bifurcation points at various temperatures for TAME system (P=2.55 atm).

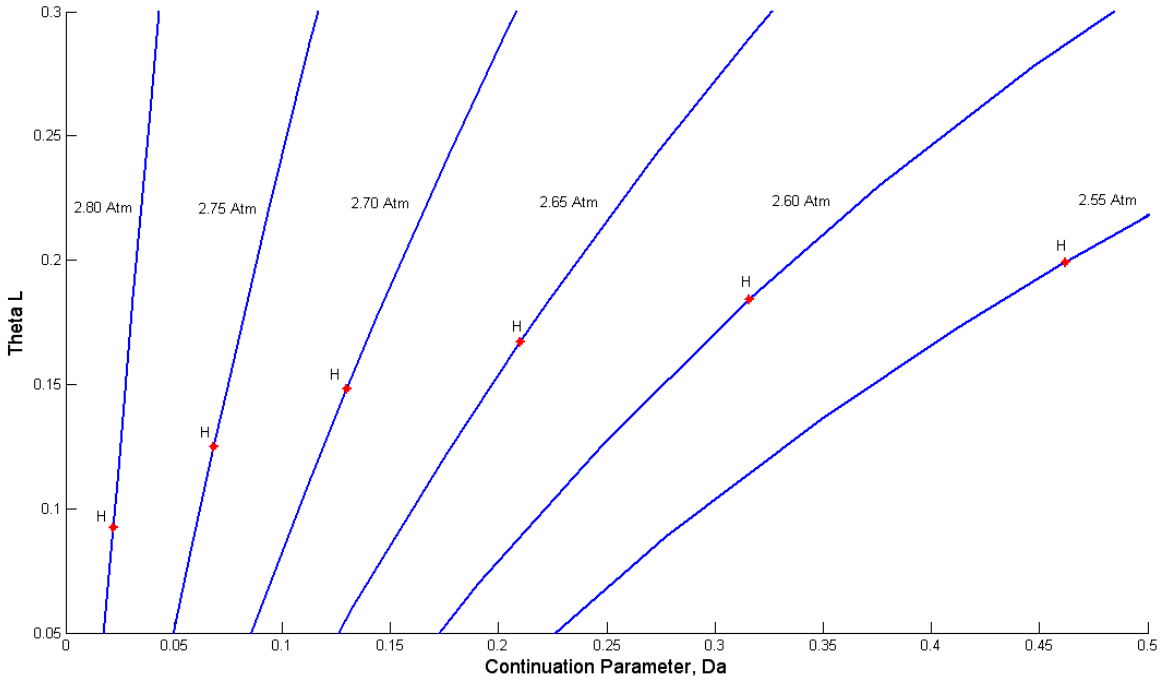

Figure 4-10. **The behavior of the Hopf bifurcation points at various pressures for TAME system (T=335 K).**

4.8 Discussion of Results

Results obtained clearly demonstrate the existence of Hopf bifurcations which causes the coexistence of a stable steady state and an unstable limit cycle in isothermal reactive flash processes. It is possible that, under certain operating conditions, these Hopf bifurcations can exist in multistage columns too, and such columns may need special control mechanisms such as delayed feedback control. Mohl et al.[26] showed that an isothermal CSTR problem involving the MTBE and TAME reactions cannot exhibit Hopf bifurcations. The work of Lucia[45] clearly shows that an isothermal non-reactive flash problem cannot exhibit any multiple steady states. Furthermore, as can be seen in Figure 4-1, at large Damköhler numbers these bifurcation points do not exist.

Therefore, we conclude that it is the combination of the phase equilibrium and the reaction that causes these Hopf bifurcations. Just as two nonsingular Jacobian matrixes can be added/combined to give a singular Jacobian matrix, so also two processes that cannot by themselves produce limit cycles can be combined to produce highly nonlinear phenomenon like Hopf bifurcations. Additionally, this paper demonstrates that such instabilities and oscillations are not necessarily due to multiple stages and can occur even in isothermal reactive separation process problems.

4.9 Conclusions

The main conclusions of this Chapter are as follows.

- The Rachford-Rice procedure used to solve non-reactive flash isothermal isobaric flash processes can be extended to reactive systems.
- While isothermal CSTR problems and isothermal non-reactive flash problems do not exhibit Hopf bifurcations, isothermal reactive flash process problems involving MTBE and TAME mixtures do exhibit Hopf bifurcations.
- In the neighborhood of these Hopf bifurcations, both limit cycles and steady-states can be observed.

Chapter 5 Singularities in Non-Equilibrium Reactive Separation Processes

In this chapter, we demonstrate the existence of various types of singularities in equilibrium and non-equilibrium reactive separation process problems. First, the equilibrium reactive separation process problem is posed as a set of differential algebraic equations (DAE) and it is shown that Hopf bifurcation points can exist even for this formulation, for both the MTBE and TAME systems as in Ruiz et al.[52]. Extension of this analysis to non-equilibrium models shows the existence of limit points in the case of the TAME mixture and isolas with intersecting branches in the case of the MTBE mixture.

5.1 Introduction

Multiple steady-states in non-equilibrium reactive distillations was demonstrated by several workers[1, 3, 53-56] but all this work involve RD multistage columns. In a recent article Ruiz et al.[52] analyzed the isothermal isobaric reactive flash problem and showed that the MTBE reactive flash process, under isothermal isobaric conditions exhibited Hopf bifurcations. In this article we modify the approach used by Ruiz et al.[52], where a continuation procedure implemented in CL_MATCONT was used to solve all the equations for the reactive flash taken together. In this chapter, we express the reactive flash problem as a set of differential algebraic equation system (DAE) and demonstrate Hopf bifurcations for the MTBE and TAME systems even when such an approach is used. We then investigate the nature of the singularities in the non-equilibrium reactive isothermal flash problem described in Sridhar et al.[17] and show that

the effect of imposing mass transfer rate equations on the equilibrium reactive flash problem causes the emergence of singularities like limit points and bifurcation (branch) points. This chapter is organized as follows; first the DAE formulation for the equilibrium reactive flash process is described. Then we demonstrate the solution procedure and the existence of Hopf bifurcations for the MTBE and TAME isothermal reactive flash problems. We then implement a similar procedure for the non-equilibrium isothermal and non-isothermal reactive flash problems and show the existence of limit points in the case of the TAME mixture and bifurcation points and isolas in the case of the MTBE system.

5.2 DAE Formulation for the Isothermal Isobaric Equilibrium Reactive Flash Problem

The differential algebraic formulation for the isothermal isobaric reactive flash problem can be derived as follows.

Equation (4.1) can be re-written as

$$\frac{dx_i}{d\tau} = z_i - \theta_V y_i - \theta_L x_i + \frac{\mathrm{Da}}{k_{f,\mathrm{ref}}}\left(v_i R\right) \tag{5.1}$$

while the overall mass balance equation is

$$1 - \theta_V - \theta_L + \frac{\mathrm{Da}}{k_{f,\mathrm{ref}}}\left(v_T R\right) = 0 \tag{5.2}$$

The summation expression for the vapor phase (equation (4.5)) and the phase equilibrium relation (equation (4.3)), can be combined to yield $\sum_{i=1}^{n} K_i x_i = 1$ which by differentiation with time will yield

$$\sum_{i=1}^{n} K_i \frac{dx_i}{d\tau} + \sum_{i=1}^{n} x_i \frac{dK_i}{d\tau} = 0 \tag{5.3}$$

Since, $K_i = \frac{P_i^{\text{sat}}}{P}\gamma_i$, $\frac{dK_i}{d\tau} = \frac{P_i^{\text{sat}}}{P}\frac{d\gamma_i}{d\tau}$ and applying the chain rule to $\frac{d\gamma_i}{d\tau}$

we take

$$\frac{d\gamma_i}{d\tau} = \sum_{j=1}^{n} \frac{\partial \gamma_i}{\partial x_j}\frac{dx_j}{d\tau} \tag{5.4}$$

and this would yield the equations

$$\frac{dK_i}{d\tau} = \frac{P_i^{\text{sat}}}{P}\sum_{j=1}^{n} \frac{\partial \gamma_i}{\partial x_j}\frac{dx_j}{d\tau} \tag{5.5}$$

and

$$\sum_{i=1}^{n} K_i \frac{dx_i}{d\tau} + \frac{1}{P}\sum_{i=1}^{n} P_i^{\text{sat}} \sum_{j=1}^{n} x_i \frac{\partial \gamma_i}{\partial x_j}\frac{dx_j}{d\tau} = 0 \tag{5.6}$$

Expressing $\frac{\partial \gamma_i}{\partial x_j}$ in logarithmic form, we take $\frac{\partial \gamma_i}{\partial x_j} = \gamma_i \frac{\partial \ln \gamma_i}{\partial x_j}$ and substitution yields

$$\sum_{i=1}^{n} K_i \frac{dx_i}{d\tau} + \frac{1}{P}\sum_{i=1}^{n} P_i^{\text{sat}} \sum_{j=1}^{n} \gamma_i \left(x_i \frac{\partial \ln \gamma_i}{\partial x_j} \right) \frac{dx_j}{d\tau} = 0 \tag{5.7}$$

Substitution of the component mass balance equation yields

$$\begin{aligned} &\sum_{i=1}^{n} K_i \left(z_i - \theta_V y_i - \theta_L x_i + \frac{\text{Da}}{k_{f,\text{ref}}} v_i R \right) \\ &+ \frac{1}{P}\sum_{i=1}^{n} \left(P_i^{\text{sat}} \sum_{j=1}^{n} \gamma_i \left(x_i \frac{\partial \ln \gamma_i}{\partial x_j} \right) \left(z_j - \theta_V y_j - \theta_L x_j + \frac{\text{Da}}{k_{f,\text{ref}}} v_j R \right) \right) = 0 \end{aligned} \tag{5.8}$$

Grouping similar terms for θ_L and θ_V

$$\sum_{i=1}^{n} K_i \left(z_i + \frac{\mathrm{Da}}{k_{f,\mathrm{ref}}} v_i R \right) + \sum_{i=1}^{n} \left(\frac{P_i^{\mathrm{sat}} \gamma_i}{P} \sum_{j=1}^{n} \left(x_i \frac{\partial \ln \gamma_i}{\partial x_j} \right) \left(z_j + \frac{\mathrm{Da}}{k_{f,\mathrm{ref}}} v_j R \right) \right)$$
$$-\theta_L \left(\sum_{i=1}^{n} K_i x_i + \sum_{i=1}^{n} \left(\frac{P_i^{\mathrm{sat}} \gamma_i}{P} \sum_{j=1}^{n} \left(x_i \frac{\partial \ln \gamma_i}{\partial x_j} \right) x_j \right) \right) \tag{5.9}$$
$$-\theta_V \left(\sum_{i=1}^{n} K_i y_i + \sum_{i=1}^{n} \left(\frac{P_i^{\mathrm{sat}} \gamma_i}{P} \sum_{j=1}^{n} \left(x_i \frac{\partial \ln \gamma_i}{\partial x_j} \right) y_j \right) \right) = 0$$

or

$$\sum_{i=1}^{n} K_i \left(z_i + \frac{\mathrm{Da}}{k_{f,\mathrm{ref}}} v_i R + \sum_{j=1}^{n} \left(x_i \frac{\partial \ln \gamma_i}{\partial x_j} \right) \left(z_j + \frac{\mathrm{Da}}{k_{f,\mathrm{ref}}} v_j R \right) \right)$$
$$-\theta_L \left(\sum_{i=1}^{n} K_i \left(x_i + \sum_{j=1}^{n} \left(x_i \frac{\partial \ln \gamma_i}{\partial x_j} \right) x_j \right) \right) - \theta_V \left(\sum_{i=1}^{n} K_i \left(y_i + \sum_{j=1}^{n} \left(x_i \frac{\partial \ln \gamma_i}{\partial x_j} \right) y_j \right) \right) = 0 \tag{5.10}$$

Furthermore, since $\theta_L = 1 - \theta_V + \frac{\mathrm{Da}}{k_{f,\mathrm{ref}}} \left(v_T R \right)$ we would get

$$\sum_{i=1}^{n} K_i \left(z_i + \frac{\mathrm{Da}}{k_{f,\mathrm{ref}}} v_i R + \sum_{j=1}^{n} \left(x_i \frac{\partial \ln \gamma_i}{\partial x_j} \right) \left(z_j + \frac{\mathrm{Da}}{k_{f,\mathrm{ref}}} v_j R \right) \right) - \left(1 - \theta_V + \frac{\mathrm{Da}}{k_{f,\mathrm{ref}}} v_T R \right)$$
$$\left(\sum_{i=1}^{n} K_i \left(x_i + \sum_{j=1}^{n} \left(x_i \frac{\partial \ln \gamma_i}{\partial x_j} \right) x_j \right) \right) - \theta_V \left(\sum_{i=1}^{n} K_i \left(y_i + \sum_{j=1}^{n} \left(x_i \frac{\partial \ln \gamma_i}{\partial x_j} \right) y_j \right) \right) = 0 \tag{5.11}$$

We can then solve for θ_V as

$$\theta_V = \frac{\left(1 + \frac{\mathrm{Da}}{k_{f,\mathrm{ref}}} v_T R \right) \left(\sum_{i=1}^{n} K_i \left(x_i + \sum_{j=1}^{n} \left(x_i \frac{\partial \ln \gamma_i}{\partial x_j} \right) x_j \right) \right) - \sum_{i=1}^{n} K_i \left(z_i + \frac{\mathrm{Da}}{k_{f,\mathrm{ref}}} v_i R + \sum_{j=1}^{n} \left(x_i \frac{\partial \ln \gamma_i}{\partial x_j} \right) \left(z_j + \frac{\mathrm{Da}}{k_{f,\mathrm{ref}}} v_j R \right) \right)}{\sum_{i=1}^{n} K_i \left(x_i - y_i + \sum_{j=1}^{n} \left(x_i \frac{\partial \ln \gamma_i}{\partial x_j} \right) \left(x_j - y_j \right) \right)} \tag{5.12}$$

which can be simplified into

$$\theta_V = \sum_{i=1}^{n} \left(\frac{\left(1+\frac{\mathrm{Da}}{k_{f,\mathrm{ref}}} v_T R\right)\left(x_i + \sum_{j=1}^{n}\left(x_i \frac{\partial \ln \gamma_i}{\partial x_j}\right) x_j\right) - z_i - \frac{\mathrm{Da}}{k_{f,\mathrm{ref}}} v_i R - \sum_{j=1}^{n}\left(x_i \frac{\partial \ln \gamma_i}{\partial x_j}\right)\left(z_j + \frac{\mathrm{Da}}{k_{f,\mathrm{ref}}} v_j R\right)}{x_i - y_i + \sum_{j=1}^{n}\left(x_i \frac{\partial \ln \gamma_i}{\partial x_j}\right)\left(x_j - y_j\right)} \right)$$

(5.13)

Equation (5.2) can be rewritten as

$$\theta_L = 1 - \theta_V + \frac{\mathrm{Da}}{k_{f,\mathrm{ref}}}\left(v_T R\right) \tag{5.14}$$

and therefore the DAE equation set for the reactive flash are equation (5.13), (5.14), (4.3) and (5.1).

For a given temperature, pressure, feed composition, Damköhler number, and an initial guess for the liquid phase composition we can calculate the vapor phase composition, activity coefficient, evaluate θ_L and θ_V, and solve the differential equation (5.1) at steady state. The initial solution point is then fed into CL_MATCONT (section 3.2) to obtain the solution curve.

5.3 Non Equilibrium Reactive Model

The non-equilibrium model has separate balance equations for each phase, which are interconnected by material and energy balances around the interphase. The energy balance is one for each phase, each one containing a rate of energy transfer term across bulk interphase.

A schematic representation of the non-equilibrium reactive stage is shown in Figure 5-1. The component molar balance equations for the vapor and liquid phase are:

$$\frac{d\varepsilon_{i,j}^{V}}{dt} = f_{i,j}^{V} - V_j y_{i,j} + V_{j+1} y_{i,j+1} - N_{i,j}^{V} a_{\text{net}\,j} \tag{5.15}$$

$$\frac{d\varepsilon_{i,j}^{L}}{dt} = f_{i,j}^{L} - L_j x_{i,j} + L_{j-1} x_{i,j-1} + N_{i,j}^{L} a_{\text{net}\,j} + \varepsilon_j \sum_{m=1}^{r} \nu_{i,m} R_{m,j} \tag{5.16}$$

$R_{m,j}$ is the rate of reaction m on stage j, $a_{\text{net}\,j}$ is the net interfacial area on stage j, ε_j the reaction holdup, and $N_{i,j}$ represents the interface mass transfer rate for the component i on stage j that is related to the chemical potential gradients in either phase by the generalized Maxwell Stefan equations

$$\frac{x_{i,j}}{\mathbb{R}T_j^{L}} \frac{\partial \mu_{i,j}^{L}}{\partial \eta} = \sum_{k=1}^{c} \frac{x_{i,j} N_{k,j}^{L} - x_{k,j} N_{i,j}^{L}}{c_{t,j}^{L} \left(k_{i,k}^{L} a_{\text{net}} \right)_j} \tag{5.17}$$

$$\frac{y_{i,j}}{\mathbb{R}T_j^{V}} \frac{\partial \mu_{i,j}^{v}}{\partial \eta} = \sum_{k=1}^{c} \frac{y_{i,j} N_{k,j}^{v} - y_{k,j} N_{i,j}^{v}}{c_{t,j}^{v} \left(k_{i,k}^{v} a_{\text{net}} \right)_j} \tag{5.18}$$

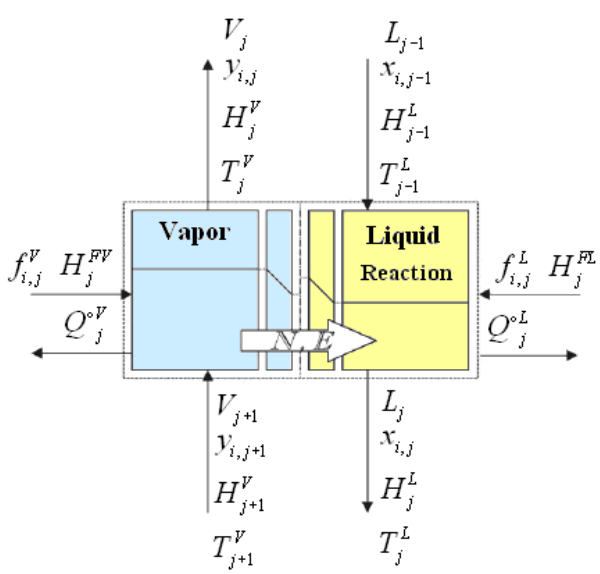

Figure 5-1. The non-equilibrium stage for homogeneous liquid-phase reaction

where $k_{i,k}$ represent the corresponding mass transfer coefficient of the *i*-*k* pair in the appropriate phase, c_t is the total concentration, $\mu_{i,j}$ is the chemical potential for the component *i* on stage *j*, $\mathbb{R}$ is the gas constant, and η is the dimensionless distance along diffusion path.

The energy balance equations,

$$\frac{d\left(H\varepsilon\right)_j^V}{dt} = F_j^V H_j^{VF} - V_j H_j^V + V_{j+1} H_{j+1}^V - E_j^V a_{\text{net}\,j} + Q^{\circ V}_j \tag{5.19}$$

$$\frac{d\left(H\varepsilon\right)_j^L}{dt} = F_j^L H_j^{LF} - L_j H_j^L + L_{j+1} H_{j+1}^L + E_j^L a_{\text{net}\,j} + Q^{\circ L}_j \tag{5.20}$$

The interface energy transfer fluxes both with conductive and convective terms

$$E_j^V = -\mathbf{h}_j^V \frac{\partial T_j^{\,V}}{\partial \eta} + \sum_{i=1}^{c} N_{i,j}^V H_{i,j}^V \tag{5.21}$$

$$E_j^L = -\mathbf{h}_j^L \frac{\partial T_j^{\,L}}{\partial \eta} + \sum_{i=1}^{c} N_{i,j}^L H_{i,j}^L \tag{5.22}$$

where $\mathbf{h}_j$ is the heat transfer coefficient in the appropriate phase on stage *j*, and $H_{i,j}$ is the molar enthalpy for the component *i* on stage *j*.

The phase equilibrium relation at the interface,

$$y_{i,j}^I = K_{i,j} x_{i,j}^I \tag{5.23}$$

The summation of vapor and liquid mole fraction at the interface,

$$\sum_{i=1}^{c} y_{i\ j}^I = 1 \tag{5.24}$$

$$\sum_{i=1}^{c} x_{i\ j}^I = 1 \tag{5.25}$$

5.4 Non-Equilibrium Reactive Flash Problem

The motivation of analyzing the non-equilibrium reactive TP problem is to investigate the effect of the mass transfer equations on the single stage reactive flash problem. Consequently we look at a reactive analog of the single stage non-equilibrium flash problem described in Sridhar et al.[17]. The equations in this problem include the material balance for the vapor and liquid phase, the phase equilibrium relationships and the transfer rate equations. Assuming the reaction occurs in the liquid phase the equations are very similar to that described in Sridhar et al.[17] except for the reaction term in the liquid phase material balance equation. The equations for the single stage non-equilibrium reactive flash problem include the material balance equations for the vapor and liquid phases

$$f_i^V - Vy_i - N_i^V a_{\text{net}} = 0 \tag{5.26}$$

and

$$f_i^L - Lx_i + N_i^L a_{\text{net}} + \varepsilon^L \sum_{m=1}^{r} v_{i,m} R_m = 0 \tag{5.27}$$

The phase equilibrium relationships at the interface can be written as

$$y_i^I = K_i x_i^I \tag{5.28}$$

The transfer rate equations for the vapor and liquid phases expressed in c-1 dimensional matrix form are

$$(N^V) = c_t^V \left[\kappa^V\right]\left(y - y^I\right) + N_t^V\left(y\right) \tag{5.29}$$

$$(N^L) = c_t^L \left[\kappa^L\right]\left(x^I - x\right) + N_t^L\left(x\right) \tag{5.30}$$

The mass transfer coefficients κ^V and κ^L are calculated (Appendix A) using the AIChE method[57] with the modification of Bennett et al.[58] while the interfacial area was calculated

(Appendix B) using the procedures in Zuiderweg[59]. These procedures are also described in Taylor and Krishna[60].

The interface material balance equations would be

$$N_i^L\Big|_I - N_i^V\Big|_I = 0 \tag{5.31}$$

Additionally we have the summation equations for the interface compositions

$$\sum_{i=1}^{c} x_i^I = 1 \tag{5.32}$$

and

$$\sum_{i=1}^{c} y_i^I = 1 \tag{5.33}$$

In order to obtain the singularities in the problem we must divide this set of equations into differential and algebraic equations. The ordinary differential equations that we will incorporate in CL_MATCONT (section 3.2) are the material balance equations for the vapor and liquid phases

$$\frac{d\varepsilon_i^V}{dt} = f_i^V - Vy_i - N_i^V a_{\text{net}} \tag{5.34}$$

and

$$\frac{d\varepsilon_i^L}{dt} = f_i^L - Lx_i + N_i^L a_{\text{net}} + \text{Da}\frac{F^L}{k_{f,\text{ref}}}\sum_{m=1}^{r} v_{i,m}R_m \tag{5.35}$$

These are the two equations that will be incorporated by the CL_MATCONT program to investigate the singularities. The other equations will be the algebraic equations which will be solved along with the ordinary differential equations. Defining $\varepsilon_i^L = \varepsilon^L x_i$ and $\varepsilon_i^V = \varepsilon^V y_i$ we can rewrite equations (5.34) and (5.35) as

$$\frac{dy_i}{dt} = \frac{1}{\varepsilon^V}\left(f_i^V - Vy_i - N_i^V a_{\text{net}} \right) \tag{5.36}$$

and

$$\frac{dx_i}{dt} = \frac{1}{\varepsilon^L}\left(f_i^L - Lx_i + N_i^L a_{\text{net}} + \text{Da}\frac{F^L}{k_{f,\text{ref}}}\sum_{m=1}^{r} v_{i,m} R_m \right) \tag{5.37}$$

For a given temperature and pressure and fixed feed composition, the algebraic system of equations are first solved. This is done by first fixing an initial guess for x_i^I, y_i^I, N_i^V, N_i^L, V and L. The physical properties ρ_L, ρ_V, σ, μ_V, D_V, D_L are then estimated (Appendix A) and the tray design procedure (Appendix B) is executed. The multicomponent mass transfer coefficients are then obtained and the steady state version of the ordinary differential equation system is then solved. When the two systems of equations converge, the liquid and vapor holdups are calculated by the empirical correlations in the tray design procedure. This gives us the initial value of the Damköhler number which is used as a continuation parameter. The design parameters that constitute the tray specifications are then fixed. With these design parameters maintained constant, the continuation procedure using CL_MATCONT is then executed using the Damköhler number as the continuation parameter.

In the non-isothermal non-equilibrium case, we consider additionally the bulk energy balance equations in the liquid and vapor phase which are

$$\frac{dU^L}{dt} = F^L H^{LF} - LH^L + E^L a_{\text{net}} + Q^{\circ L} \tag{5.38}$$

$$\frac{dU^V}{dt} = F^V H^{VF} - VH^V - E^V a_{\text{net}} + Q^{\circ V} \tag{5.39}$$

where $U^L = \varepsilon^L H^L$, $U^V = \varepsilon^V H^V$, and Q° is the heat transfer rate from the surroundings.

We also consider the interface energy balance equation

$$E^L\Big|_I - E^V\Big|_I = 0 \tag{5.40}$$

The energy fluxes, which include the convective and conductive contributions, are

$$E^L = \mathbf{h}^L\left(T^I - T^L\right) + \sum_{i=1}^{c} N_i^L H_i^L \tag{5.41}$$

$$E^V = \mathbf{h}^V\left(T^V - T^I\right) + \sum_{i=1}^{c} N_i^V H_i^V \tag{5.42}$$

The liquid and vapor heat transfer coefficients (Appendix A) are $\mathbf{h}^L = \kappa^L \rho_t^{\,L} C_p^{\,L}\,\mathrm{Le}^{1/2}$, and $\mathbf{h}^V = \kappa^V \rho_t^{\,V} C_p^{\,V}\,\mathrm{Le}^{2/3}$ where Le is the Lewis number. The enthalpies are calculated using a procedure showed in Appendix A. Figure 5-2 and Figure 5-3 show the algorithm flowcharts for the isothermal and non-isothermal non-equilibrium problems.

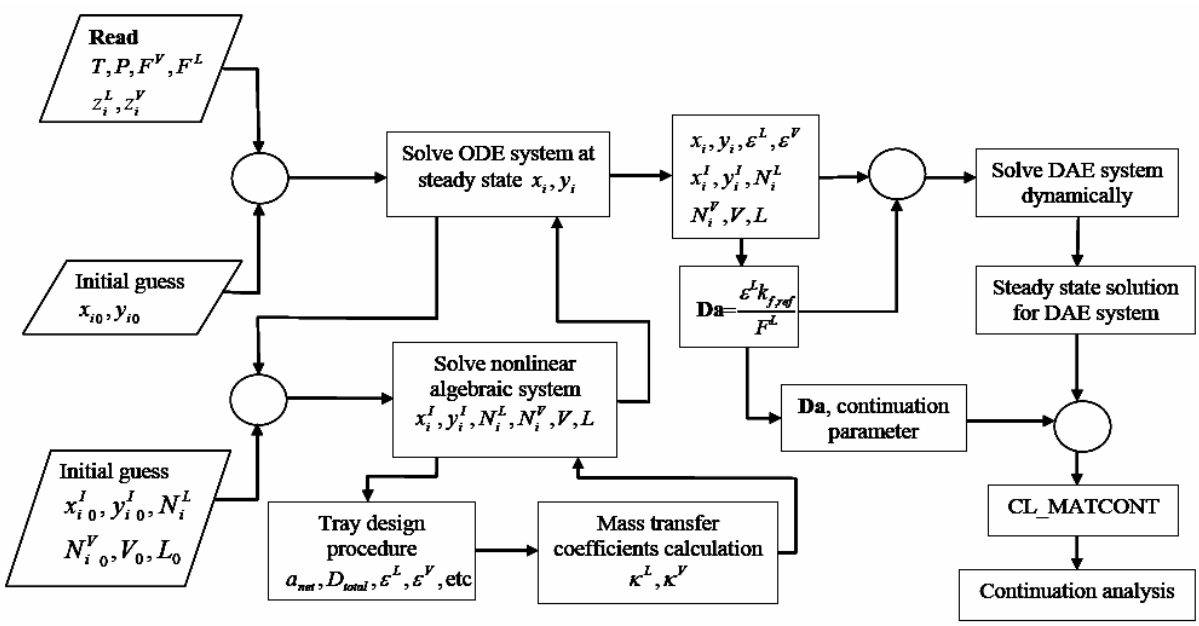

Figure 5-2. Algorithm flowchart for isothermal non-equilibrium problem.

5.5 Results and Discussion

We found singularities for both the equilibrium and non-equilibrium models for both the MTBE and TAME synthesis. The MTBE system is given in Section 2.5, and the TAME system is illustrated in Section 4.4. The DAE system solved using CL_MATCONT produced the following results. The equilibrium reactive flash problem showed the existence of Hopf bifurcations as in Ruiz et al.[52] whereas the nonequilibrium problem revealed the existence of limit points (turning points) in the case of the TAME mixture and isolas with an intersecting branch in the case of the MTBE problem. Table 5-1 to Table 5-4 show the feed conditions and specifications for the equilibrium and nonequilibrium problems. Figure 5-4 to Figure 5-9 show the solution curves with the singular points for all the problems.

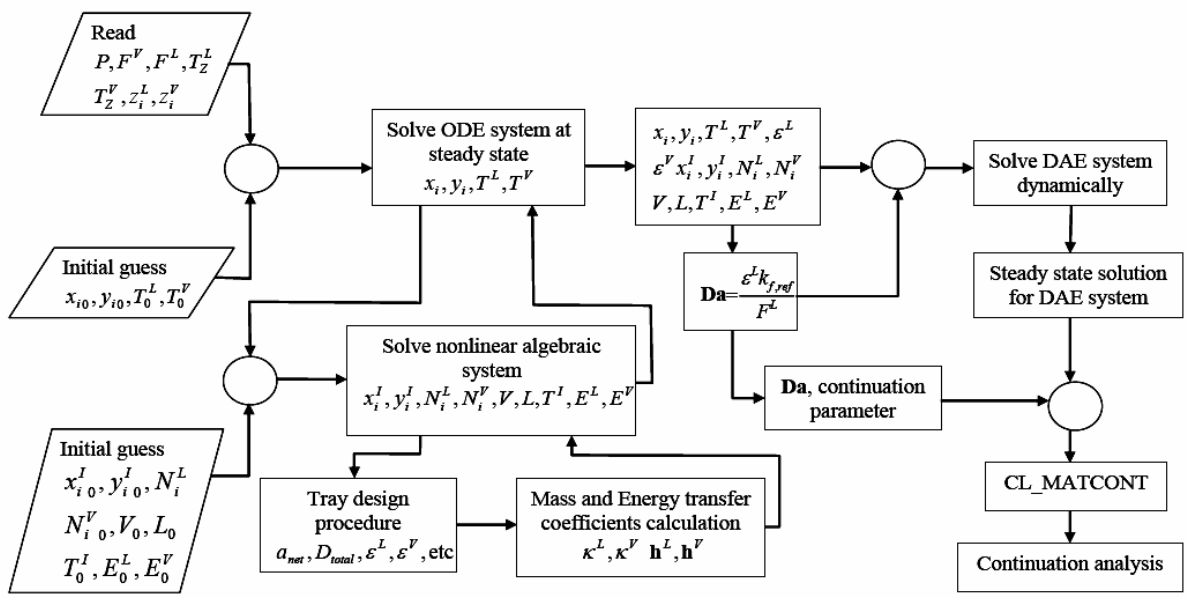

Figure 5-3. Algorithm flowchart for non-isothermal non-equilibrium problem

Two important issues can be observed from these results. First, in regard to reactive separation processes in general for non-reactive problems, Sridhar et al.[17] have shown that the imposition

of the mass-transfer equations on the equilibrium separation process problem does not cause any additional multiplicities. However, in the case of reactive separation process problems, the situation is slightly different. The imposition of the mass-transfer equations on the equilibrium reactive separation process problem cause the occurrence of limit points and branch points that are caused by the intersection of isolas with isolated branches. The additional nonlinearity that is produced by the reaction kinetics interacting with the mass transfer correlations does indeed cause the birth of the limit points and branch points.

Table 5-1. Equilibrium problem for MTBE system. Feed conditions and specifications.

Stage Specifications	
T(K)	364.25
P(bar)	11.25
$z_{Isobutene}$	0.46241
z_{MeOH}	0.08385
z_{MTBE}	0.00128
$z_{n\text{-}Butane}$	0.45245

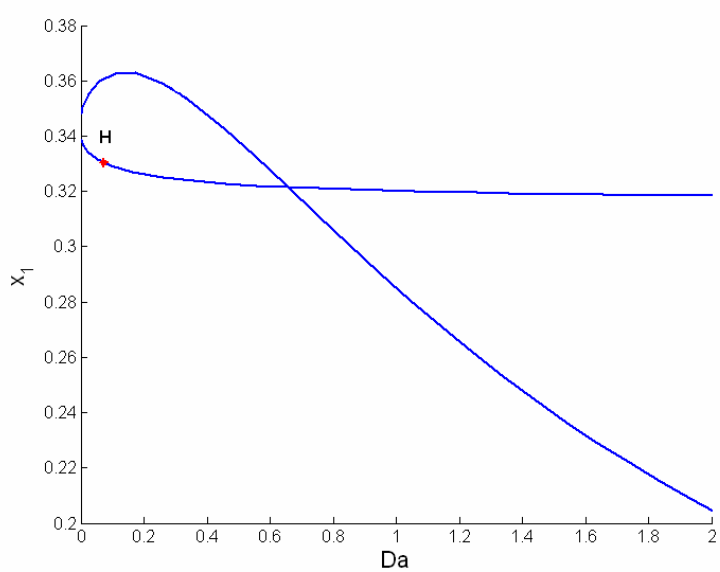

Figure 5-4. Hopf point for isothermal equilibrium MTBE problem.

Table 5-2. Equilibrium problem for TAME system. Feed conditions and specifications.

Stage Specifications	
T(K)	335
P(bar)	2.46
z_{MeOH}	0.30556
z_{2M1B}	0.03889
z_{2M2B}	0.23889
z_{TAME}	0.00000
$z_{n\text{-}Pentane}$	0.41666

The second important conclusion is the fact that the MTBE and TAME mixtures seem to react differently to the imposition of the mass-transfer equations. However, this result is not surprising to us. As far as multiple steady states are concerned, Chen et al.[4] have demonstrated that, for certain specifications, both mixtures show significantly different behavior by demonstrating that, for TAME, multiplicities are lost for high Da values, whereas for MTBE, multiplicities are lost for low Da values. This is because of the difference in kinetics in both cases. This difference in the kinetics also seems to influence the nature of the singularities that are produced by the imposition of the mass-transfer correlations on the reactive separation process problem. The MTBE process and the TAME process models do react differently when the additional mass transfer correlations are incorporated. The incorporation of the mass-transfer correlations causes the occurrence of limit (turning) points in the case of the TAME problem and branch (bifurcation) points and isolas in the case of the MTBE problem. This is due to the two different kinetic mechanism equations interacting with the mass transfer correlations.

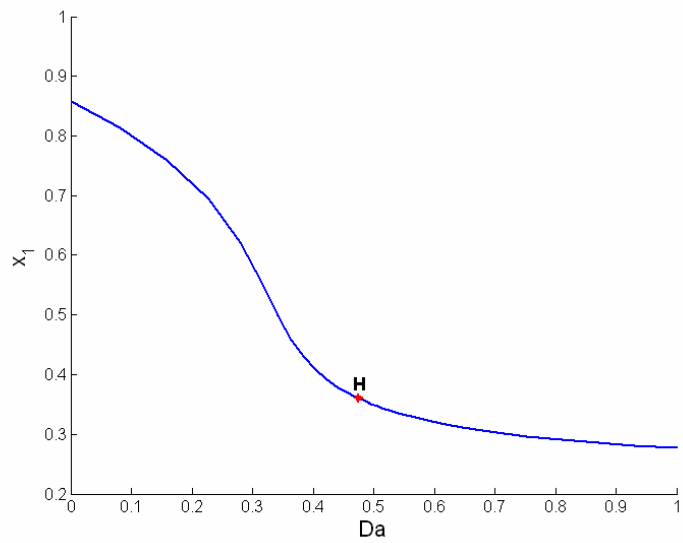

Figure 5-5. Hopf point for isothermal equilibrium TAME problem

Table 5-3. Feed conditions and specifications for nonequilibrium MTBE problem.

Stage Specifications	Liquid Phase	Vapor Phase
F(kmol/h)	216.00	252.00
T(K)	380.01	401.01
P(bar)	18.04	18.04
$z_{Isobutene}$	0.3500	0.6069
z_{MeOH}	0.3500	0.1783
z_{MTBE}	0.1980	0.0475
$z_{n\text{-}Butane}$	0.2770	0.1674

Table 5-4. Feed conditions and specifications for nonequilibrium TAME problem.

Stage Specifications	Liquid Phase	Vapor Phase
F(kmol/h)	216.00	252.00
T(K)	325.31	346.31
P(bar)	2.00	2.00
z_{MeOH}	0.090	0.197793
z_{2M1B}	0.300	0.326756
z_{2M2B}	0.350	0.302763
z_{TAME}	0.100	0.014649
$z_{n\text{-}Pentane}$	0.160	0.158039

5.6 Conclusions

This chapter investigates the nature of the singularities in equilibrium and nonequilibrium reactive separation units. It is shown that the differential algebraic equation (DAE) formulation of the equilibrium reactive separation process problem produces Hopf bifurcations such as those observed in the work of Ruiz et al.[52] It is also shown that the imposition of the mass-transfer equations on the reactive flash problem leads to the formation of limit points in the case of the TAME mixture and isolas with intersecting branches in the case of the MTBE problem.

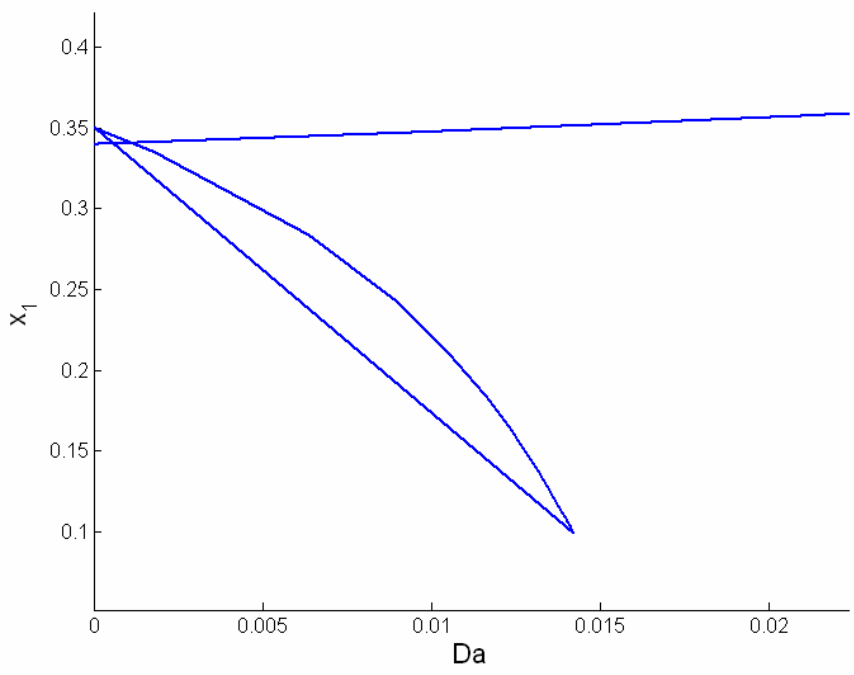

Figure 5-6. Continuation diagram for isothermal nonequilibrium MTBE problem.

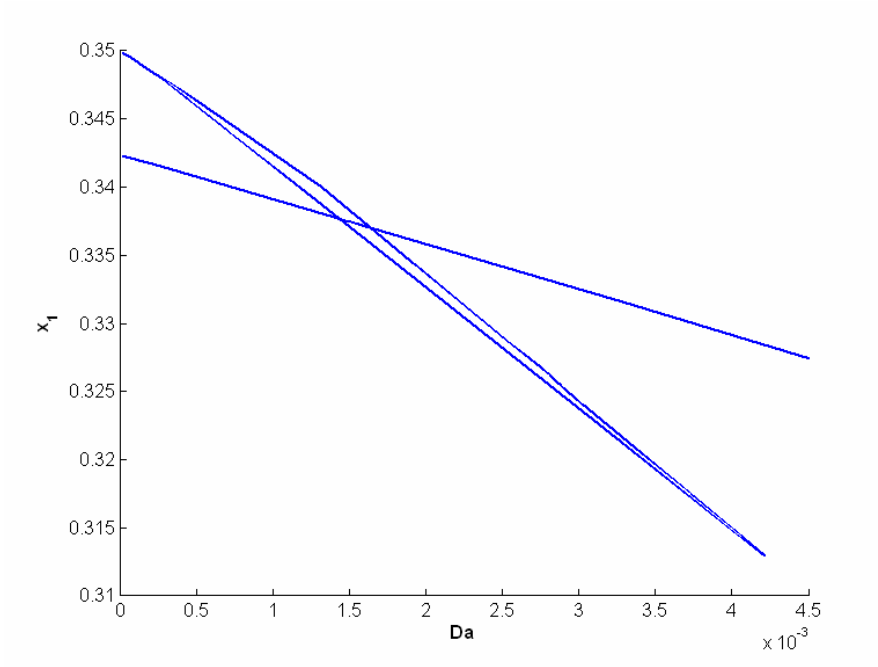

Figure 5-7. Continuation diagram for non-isothermal nonequilibrium MTBE problem.

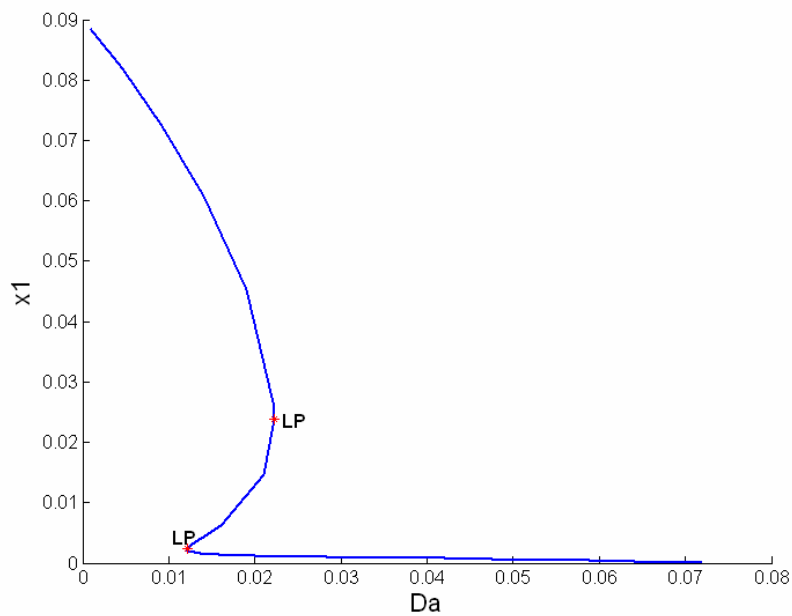

Figure 5-8. Continuation diagram for isothermal nonequilibrium TAME problem.

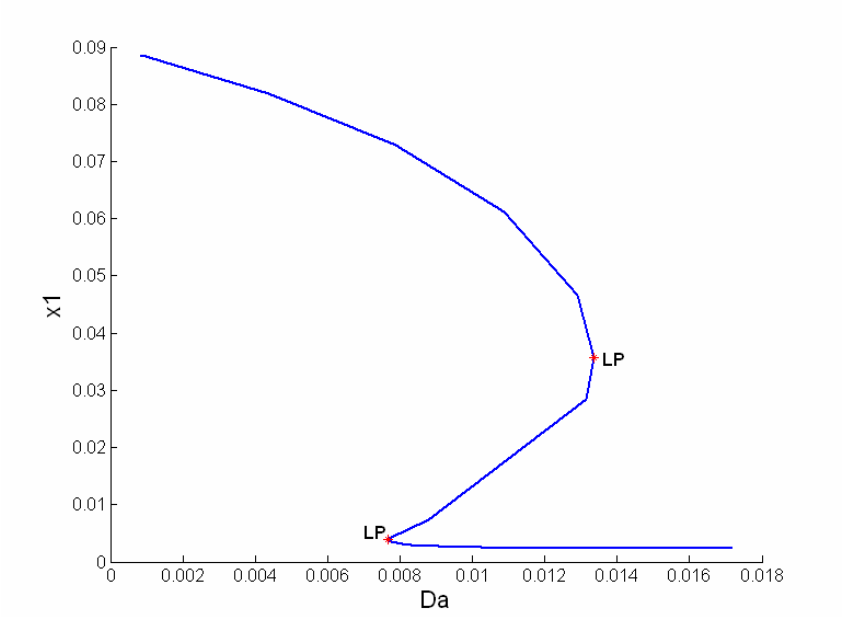

Figure 5-9. Continuation diagram for non-isothermal nonequilibrium TAME problem.

Chapter 6 Design and Analysis of Non-Equilibrium Reactive Separation Processes

In this chapter we derive new expressions to calculate the non-equilibrium residue composition maps for reactive separation processes incorporating mass transfer effects and design aspects. Next, we discuss the strategy to solve the differential algebraic equation (DAE) system to find the non-equilibrium reactive composition curve. We illustrate using the MTBE synthesis the case when stationary reactive points calculated by equilibrium and non-equilibrium approaches do not match for reactive saddle-point azeotrope. For TAME synthesis, we studied the nonequilibrium and equilibrium reactive composition curve maps in the limit of reaction equilibrium.

6.1 Introduction

The distillation residue curve maps (RCM) have been studied by several workers[5, 6, 31, 32, 46, 61-67] in the design and synthesis of reactive and non-reactive separation processes. The RCM are used to establish feasible splits by distillation of azeotropic mixtures due to the presence of nonreactive azeotropes after the reaction, reactive azeotropes, and distillation boundaries for continuous distillation at infinite reflux. In a simple distillation process the liquid composition change dynamically because the vapors are richer in the more light components than the liquid from which they came. The path of liquid compositions stating from some initial condition is called a residue curve, and the collection of all such curves for a given mixture is called a residue curve map[46]. A RCM contain the same information like a phase diagram for a mixture.

Barbosa and Doherty[5] and Ung and Doherty[6] have derived autonomous differential equations describing the dynamics of simple homogeneous reactive distillation using a set of transformed composition variables. However all these works involved the use of the equilibrium model assuming that the liquid and vapor phase composition are in equilibrium and that there are no differences between the interface and bulk composition profiles. The real reactive separation process operates distant from the physical equilibrium resulting in mass transfer fluxes between phases (non equilibrium phase) as a function of the mass transfer gradient.

Castillo and Towler[7] established a general relationship between the vapor and liquid compositions that leave a tray at total reflux condition to take into account mass transfer effect in the non reactive RCM. They assume that the behavior of a stage column could be approximated to a packed column because is has been demonstrated that residue curves represent operating liquid composition profiles of continuous packed columns at total reflux condition[65]. This approach is used by Taylor et al.[8] for the non reactive separation case to calculate equilibrium RCM and composition trajectory maps (CTM) considering mass transfer effects. Sridhar et al.[9, 10], addressed departures from equilibrium to draw composition trajectories and locate azeotropes. They conclude that the stationary points of these equations are the same, but non-equilibrium modeling is necessary to compute distillation boundaries.

This chapter is organized as follows. First, a system of equations is established and discussed to incorporate mass transfer effects and design aspects to calculate composition curve maps for reactive separation processes. Next, a strategy is established to solve the differential algebraic equation (DAE) system for the non-equilibrium reactive composition curve maps, and the case when stationary reactive points calculated by equilibrium and non-equilibrium approaches do

not match is shown for the methyl tert-butyl ether (MTBE) production. For TAME synthesis, the nonequilibrium and equilibrium reactive composition curve maps in the limit of reaction equilibrium are reported.

6.2 Derivation of the Equations

Doing a component material balance (plug flow model) for the vapor phase moving through the tray[60] (Figure 6-1):

$$\frac{dv_i}{dh} = -N_i a A_b \tag{6.1}$$

Where v_i is the molar flow rate of component i, N_i is the mass transfer flux of component i, a the interfacial area per unit volume of froth and, A_b is active bubbling area

Summing (6.1) and considering that $\sum v_i = V$,

$$\frac{dV}{dh} = -N_t a A_b \tag{6.2}$$

and $N_i = J_i^V + y_i N_t$, $v_i = y_i V$, substituting these two definitions in (6.1):

$$V\frac{dy_i}{dh} + y_i\frac{dV}{dh} = -\left(J_i^V + y_i N_t\right) a A_b \tag{6.3}$$

Substituting (6.2) in (6.3):

$$V\frac{dy_i}{dh} = -J_i^V a A_b \tag{6.4}$$

Combining (6.4) in c -1 dimensional matrix form,

$$V\frac{d\left(y\right)}{dh} = -\left(J^V\right) a A_b \tag{6.5}$$

Now, defining (J^V):

$$\left(J^V\right) = c_t^V \left[K_{OV}\right]\left(y - y^I\right) \tag{6.6}$$

where c_t^V is the total molar concentration for vapor phase, y^I the interphase vapor molar composition and, $[K_{OV}]$ the overall mass transfer coefficient matrix defined as

$$\left[K_{OV}\right]^{-1} = \left[\kappa^V\right]^{-1} + \frac{c_t^V}{c_t^L}\left[M\right]\left[\kappa^L\right]^{-1} \tag{6.7}$$

c_t^L is the total molar concentration for liquid phase, $[M]$ is the matrix of equilibrium constant $\left[M\right] = \left[K\right]\left[\Gamma\right]$, where $[K]$ is a diagonal matrix of the vapor liquid equilibrium ratios $K_i = \gamma_i P_i^S / P$, $[\Gamma]$ is the thermodynamic factor matrix (Appendix A) and, $[\kappa^V]$ and $[\kappa^L]$ are the mass transfer coefficients matrices for vapor an liquid phase respectively.

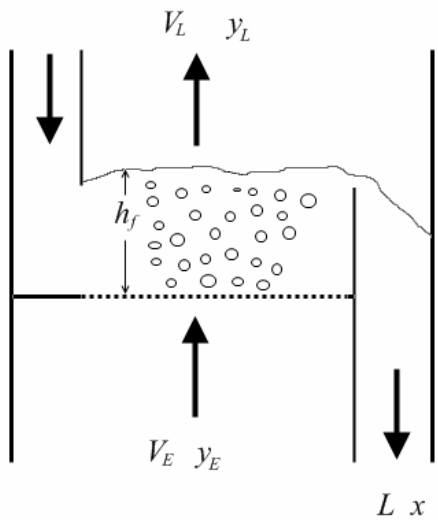

Figure 6-1. Diagram of the froth on a distillation tray.

Substituting (6.6) in (6.5)

$$\frac{d\left(y\right)}{dh} = \frac{1}{V} c_t^V \left[K_{OV}\right]\left(y^I - y\right) a A_b \tag{6.8}$$

Integrating (6.8) over the dispersion height:

$$\int_{(y_E)}^{(y_L)} \frac{d(y)}{(y^I - y)} = \int_0^{h_f} \frac{1}{V} c_t^V [K_{OV}] a A_b dh \tag{6.9}$$

$$\frac{(y^I - y_L)}{(y^I - y_E)} = \exp[-\mathbb{N}_{OV}] \tag{6.10}$$

$$(y^I - y_L) = [Q](y^I - y_E) \tag{6.11}$$

Where $[Q] = \exp[-\mathbb{N}_{OV}]$ and, $[\mathbb{N}_{OV}]$ is the overall number of transfer units for the vapor phase

$$[\mathbb{N}_{OV}] = \int_0^{h_f} \frac{1}{V} c_t^V [K_{OV}] a A_b dh \tag{6.12}$$

Rearrange (6.11)

$$(y_L) - (y^I) = [Q](y_E) - [Q](y^I) \tag{6.13}$$

Adding (y^I) and subtracting (y_E) in both sides of (6.13)

$$(y_L - y_E) = (y^I) - [Q](y^I) - (y_E) + [Q](y_E) \tag{6.14}$$

$$(y_L - y_E) = [[I] - [Q]](y^I - y_E) \tag{6.15}$$

Defining $[E] = [I]-[Q]$ then,

$$(y_L - y_E) = [E](y^I - y_E) \tag{6.16}$$

Differentiating (6.16) with respect to z, where $z = z'/D$ is the dimensionless coordinate respect to total diameter of the stage. The coordinate system is showed in Figure 6-2. Assuming the matrix $[E]$ is constant,

$$[E]\frac{d(y^I)}{dz} = \frac{d(y_L)}{dz} + [[E] - [I]]\frac{d(y_E)}{dz} \tag{6.17}$$

Assuming that $\frac{d(y_E)}{dz} = 0$, this is true for Lewis case 1[68], then (6.17) is simplified to

$$[E]\frac{d\left(y^{I}\right)}{dz}=\frac{d\left(y_{L}\right)}{dz} \tag{6.18}$$

The vapor composition at the interface is assumed in equilibrium and is related with the liquid composition trough a linear expression

$$\left(y^{*}\right)=[M](x)+(b) \tag{6.19}$$

Differentiating (6.19) with respect to z where $[M]$ and (b) are independent of z

$$\frac{d\left(y^{*}\right)}{dz}=[M]\frac{d(x)}{dz} \tag{6.20}$$

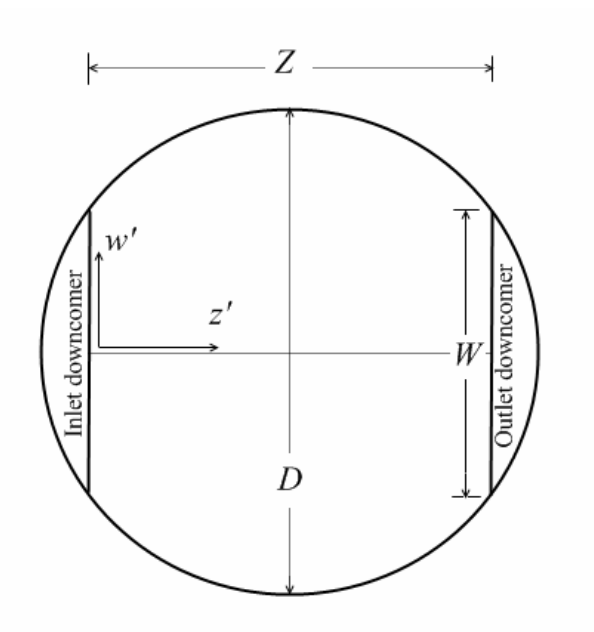

Figure 6-2. Coordinate system

Performing a material balance at steady state at any point in z' direction using Figure 9.4 in Lockett[68], and considering chemical reaction in liquid phase,

$$V'_{E}\left(y_{E}\right)dz'+L'(x)\big|_{z'+\Delta z'}-(\nu)\mathbf{R}h_{L}dz'=V'_{L}\left(y_{L}\right)dz'+L'(x)\big|_{z'} \tag{6.21}$$

Where $L'=\frac{L}{W}$, $V'=\frac{V}{A_{b}}$, (ν) is the vector of stoichiometric coefficients, and **R** is the rate of reaction. Substituting L' and V' in (6.21)

$$\frac{d(Lx)}{dz'} = \frac{V_L}{A_b} W(y)_L - \frac{V_E}{A_b} W(y)_E + Wh_L(\nu)\mathbf{R} \tag{6.22}$$

Assuming that $V = V_L = V_E$

$$L\frac{d(x)}{dz'} + \frac{dL}{dz'}(x) = V\frac{W}{A_b}(y_L - y_E) + Wh_L(\nu)\mathbf{R} \tag{6.23}$$

Doing a total mass balance

$$\frac{dL}{dz'} = Wh_L \nu_T \mathbf{R} \tag{6.24}$$

ν_T is the net stoichiometric coefficient, $\nu_T = \sum \nu_i$

Substituting (6.24) and changing *z'* to *z* in (6.23)

$$\frac{d(x)}{dz} = \frac{WD}{A_b}\frac{V}{L}(y_L - y_E) + \frac{WDh_L\mathbf{R}}{L}(\nu - \nu_T x) \tag{6.25}$$

Substituting (6.24) in (6.20)

$$\frac{d(y^*)}{dz} = [M]\left(\frac{WD}{A_b}\frac{V}{L}(y_L - y_E) + \frac{WDh_L\mathbf{R}}{L}(\nu - \nu_T x)\right) \tag{6.26}$$

Replacing (6.26) in (6.18)

$$\frac{d(y_L)}{dz} = \frac{WD}{A_b}[E][\Lambda](y_L - y_E) + \frac{WDh_L\mathbf{R}}{V}[E][\Lambda](\nu - \nu_T x) \tag{6.27}$$

Where $[\Lambda] = \frac{V}{L}[M]$

At total reflux condition $y_E = x$, and *x* is independent of y_L and *z*.

Defining $(Y_L) = (y_L - y_E)$, $A = \frac{WD}{A_b}$, $B = \frac{WDh_L\mathbf{R}}{V}$ and substituting in (6.27)

$$\frac{d(Y_L)}{dz} = A[E][\Lambda](Y_L) + B[E][\Lambda](\nu - \nu_T x) \tag{6.28}$$

Solving (6.28) as a first order linear equation with $(Y_L)=(Y_{L0})$ at $z=0$ as initial conditions, where $(Y_{L0})=(y_{L0}-y_E)$ and y_{L0} is the composition of the vapor above the liquid at the tray exit ($z=0$)

$$(Y_L)=\frac{B}{A}\left[\exp\left[A[E][\Lambda]z\right]-[I]\right](\nu-\nu_T x)+\exp\left[A[E][\Lambda]z\right](Y_{L0}) \tag{6.29}$$

Defining $(\overline{Y}_L)$ as the average vapor composition above the liquid, $(\overline{Y}_L)=(\overline{y}_L-y_E)$

$$(\overline{Y}_L)=\int_0^1 (Y_L)\,dz \tag{6.30}$$

Combining (6.29) with (6.30) and solving

$$(\overline{Y}_L)=\frac{B}{A}\left[\left[\exp\left[[E][\Lambda']\right]-[I]\right][\Lambda']^{-1}[E]^{-1}-[I]\right](\nu-\nu_T x)+\left[\exp\left[[E][\Lambda']\right]-[I]\right][\Lambda']^{-1}[E]^{-1}(Y_{L0}) \tag{6.31}$$

Where $[\Lambda']=A[\Lambda]$. Defining $\left[E^{MV}{}'\right]$ as a square matrix ((c-1)×(c-1)) of multicomponent Murphree tray efficiencies relative to $[\Lambda']$

$$\left[E^{MV}{}'\right]=\left[\exp\left[[E][\Lambda']\right]-[I]\right][\Lambda']^{-1} \tag{6.32}$$

If A=1 that is for a rectangular tray of width W and length Z, equation (6.32) is the same expression of multicomponent Murphree tray efficiencies defined by Taylor and Krishna[60].

Substituting (6.32) in (6.31)

$$(\overline{Y}_L)=\frac{B}{A}\left[\left[E^{MV}{}'\right][E]^{-1}-[I]\right](\nu-\nu_T x)+\left[E^{MV}{}'\right][E]^{-1}(Y_{L0}) \tag{6.33}$$

Rewriting (6.33) in terms of $\overline{y}_L$, y_{L0} and y_E

$$(\overline{y}_L-y_E)=\frac{B}{A}\left[\left[E^{MV}{}'\right][E]^{-1}-[I]\right](\nu-\nu_T x)+\left[E^{MV}{}'\right][E]^{-1}(y_{L0}-y_E) \tag{6.34}$$

Using (6.16) with $y^I=y_0^*$ in (6.34)

$$\left(\overline{y}_L - y_E\right) = \frac{B}{A}\left[\left[E^{MV}\,'\right]\left[E\right]^{-1} - \left[I\right]\right]\left(\nu - \nu_T x\right) + \left[E^{MV}\,'\right]\left(y_0^* - y_E\right) \tag{6.35}$$

Again, at total reflux condition $\left(x\right) = \left(y_E\right)$ and $\left(y^*\right) = \left[K\right]\left(x\right)$, equation (6.35) can be expressed as,

$$\left(\overline{y}_L\right) = \frac{B}{A}\left[\left[E^{MV}\,'\right]\left[E\right]^{-1} - \left[I\right]\right]\left(\nu - \nu_T x\right) + \left[\left[I\right] + \left[E^{MV}\,'\right]\left[K\right] - \left[E^{MV}\,'\right]\right]\left(x\right) \tag{6.36}$$

The second term in the right of (6.36) is the c -1 dimensional matrix form of equation 14 in Castillo and Towler[7].

Now, using the transformed composition variables X and Y , and the representation of residue curve maps in the transformed composition variables[6],

$$X_i = \frac{x_i - \left(\nu_i\right)\left[\nu_{\text{Ref}}\right]^{-1}\left(x_{\text{Ref}}\right)}{1 - \left(\nu_T\right)\left[\nu_{\text{Ref}}\right]^{-1}\left(x_{\text{Ref}}\right)} \qquad i = 1,\ldots,c-R \tag{6.37}$$

$$Y_i = \frac{y_i - \left(\nu_i\right)\left[\nu_{\text{Ref}}\right]^{-1}\left(y_{\text{Ref}}\right)}{1 - \left(\nu_T\right)\left[\nu_{\text{Ref}}\right]^{-1}\left(y_{\text{Ref}}\right)} \qquad i = 1,\ldots,c-R \tag{6.38}$$

$$\frac{dX_i}{d\tau} = X_i - Y_i \qquad i = 1,\ldots,c-R-1 \tag{6.39}$$

Where $\left[\nu_{\text{Ref}}\right]^{-1}$ is the inverse of the square matrix of stoichiometric coefficients for the R reference components in the R reactions,

$$\left[\nu_{\text{Ref}}\right] = \begin{bmatrix} \nu_{(c-R+1)1} & \cdots & \nu_{(c-R+1)R} \\ \vdots & \nu_{ir} & \vdots \\ \nu_{c1} & \cdots & \nu_{cR} \end{bmatrix}$$

$\left(x_{\text{Ref}}\right)$ and $\left(y_{\text{Ref}}\right)$ are column vectors of dimension R,

$$\left(x_{\text{Ref}}\right) = \begin{pmatrix} x_{c-R+1} \\ \vdots \\ x_c \end{pmatrix},\ \left(y_{\text{Ref}}\right) = \begin{pmatrix} y_{c-R+1} \\ \vdots \\ y_c \end{pmatrix}$$

(ν_i) and (ν_T) are row vectors of dimension *R*,

$$(\nu_i) = (\nu_{i1}, \nu_{i2}, \cdots, \nu_{iR}),\ (\nu_T) = (\nu_{T1}, \nu_{T2}, \cdots, \nu_{TR})$$

The transformed molar fractions satisfied the summation equations,

$$\sum_{i=1}^{c-R} X_i = 1 \tag{6.40}$$

$$\sum_{i=1}^{c-R} Y_i = 1 \tag{6.41}$$

The temperature of the system is given by the thermodynamic reaction equilibrium equation,

$$K_R = \prod_{i=1}^{c} (\gamma_i x_i)^{\nu_i} \tag{6.42}$$

Where the reaction equilibrium constant K_R is given by

$$K_R = \exp\left[-\frac{\Delta G_R^{\circ}(T)}{RT}\right] \tag{6.43}$$

6.3 Solution Strategy

To obtain the non-equilibrium composition maps, it is necessary to solve a system of differential and algebraic equations (DAE). The algorithm B in Ung and Doherty[32] is used, but is modified in the way that the relation between *y* and *x* described by equation (6.36) is used. This increases the number of algebraic equations because now *y*, *V*, and *L* appears as implicit variables. The thermodynamic factor matrix [Γ] is calculated with the Wilson model, the vapor and liquid mass transfer coefficients, and the interfacial area A_{net} are obtained as described in Ruiz et al.[69]. An important issue is the couplings of design aspects into the NEQ composition curve maps. These design aspects appear summarized in Table 6-1. They were calculated for

the MTBE and TAME non-equilibrium reactive separation processes[69]. All variables and properties are changing dynamically. Finally, the equilibrium residue curve maps are obtained with the original algorithm B[32].

Table 6-1. Tray specifications

System	MTBE	TAME
Tray type	Sieve	Sieve
Weir height (h_w)	0.092 m	0.092 m
Downcomer area (A_d)	0.047 m^2	0.041 m^2
Bubbling area (A_b)	0.50 m^2	0.93 m^2
Total tray area	0.60 m^2	1.00 m^2
Weir length (W)	0.59 m	0.62 m
Downcomer width (W_d)	0.11 m	0.09 m
Liquid flow path length (Z)	0.65 m	0.95 m
Hole pitch (p)	0.015 m	0.015 m
Hole diameter (d_h)	0.005 m	0.005 m

6.4 Case of Study 1: MTBE

The MTBE synthesis (section 2.5) is used as a case of study to draw the equilibrium and non equilibrium curve maps using the equilibrium thermodynamic data shown in Table 3.3 in Barbosa[31]. The reaction is given by the equation (6.44)

$$\underset{(c1)}{i\text{-butene}} + \underset{(c2)}{\text{MeOH}} \rightleftharpoons \underset{(c3)}{\text{MTBE}} \tag{6.44}$$

with the presence of n-butane (c4) as inert. The reference component $\left(z_{\text{Ref}}\right)$ is the MTBE and the vector of stoichiometric coefficients are $\nu = \left[-1;-1;+1;0\right]$ and $\nu_T = -1$.

Using equation (6.37) the transformed composition variables are obtained:

$$X_1 = \frac{x_1 + x_3}{1 + x_3} \tag{6.45}$$

$$X_2 = \frac{x_2 + x_3}{1 + x_3} \tag{6.46}$$

$$X_4 = \frac{x_4 + x_3}{1 + x_4} \tag{6.47}$$

The equilibrium and non-equilibrium residue composition maps for MTBE synthesis at P= 11 atm are shown in Figure 6-3. The composition map is a triangle where each corner represent a pure component of the system and each side of the triangle represent a binary mixture, two non reactive (n-butane – methanol and n-butane – *i*-butene) and one reactive (methanol – *i*-butene).

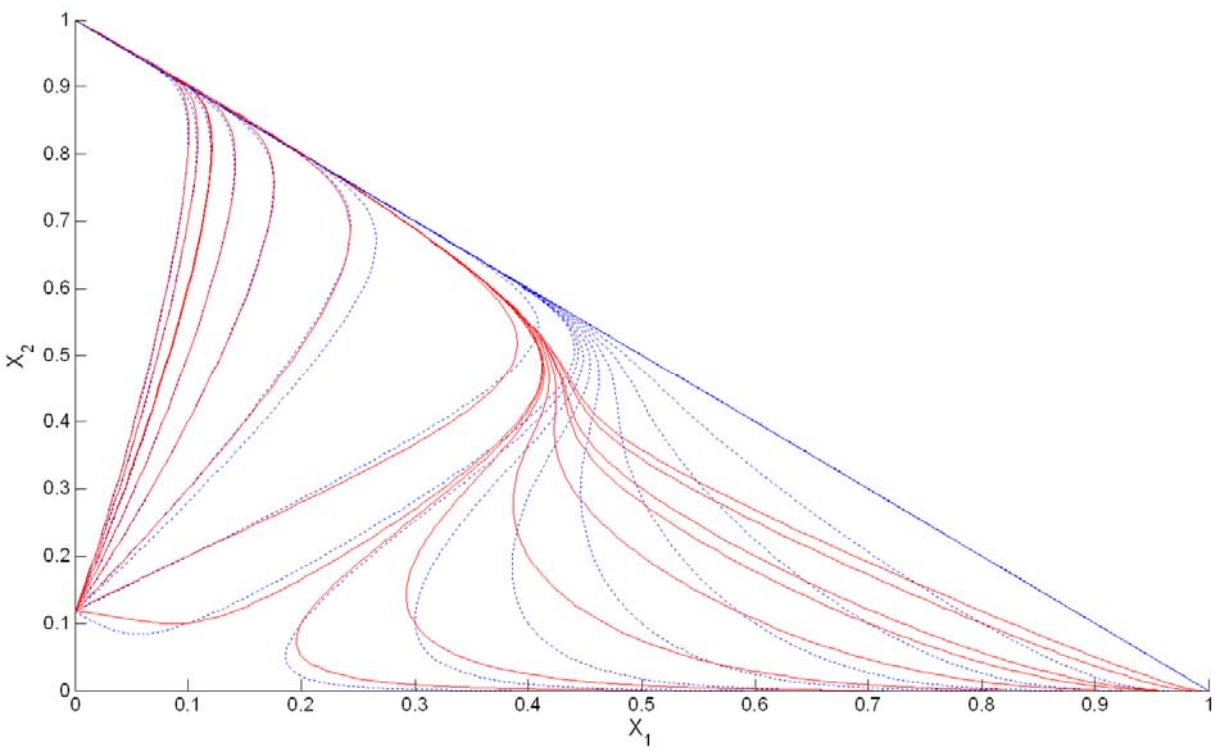

Figure 6-3. Non-equilibrium reactive composition curves (solid red lines) and equilibrium reactive composition curves (dashed blue lines) in transformed composition variables for MTBE synthesis.

The two types of models localize one non-reactive azeotrope at T=354.27 K in the n-butane – methanol axis that remain after the reaction. The convergences of these two models do not take place for another stationary point: the pseudo-reactive azeotrope as shown in phase diagram (see Figure 6-4). This azeotrope appears in the middle of the reactive vertex. For all practical purposes it is not possible to separate beyond this point and the pseudo-reactive azeotrope has the same behavior as a reactive azeotrope[32].

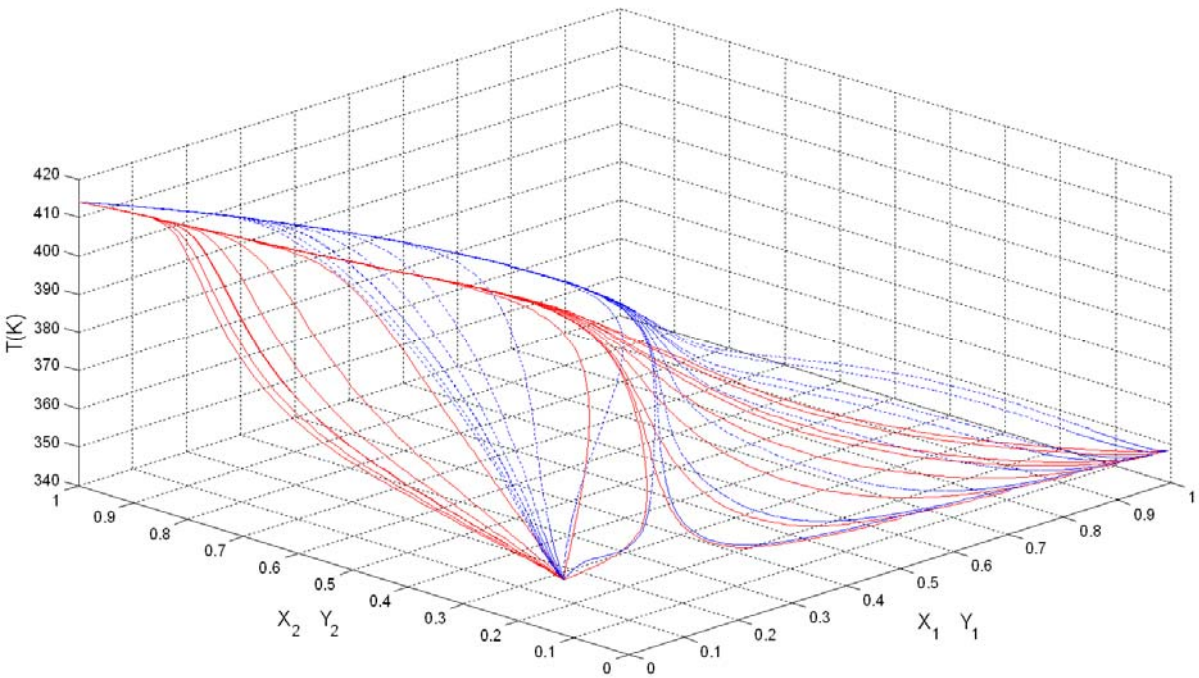

Figure 6-4. Phase diagram in transformed composition variables with temperature for MTBE synthesis at P = 11 atm (liquid phase: solid red lines, vapor phase: dashed blue lines).

When the derivative part of the DAE system is set equal to zero (steady state condition) the system is solved as a nonlinear algebraic equation system. In this study we found a reactive saddle point azeotrope in the vicinity of the n-butane vertex using the EQ and NEQ models but as it occurs in the other reactive stationary point the two models do not converge on the same composition and temperature values. Table 6-2 shows the azeotrope point coordinates for both models. The presence of the reactive saddle-point azeotrope explains why the first (in

ascendant order) residue curve originated in the non-reactive azeotrope point (Figure 6-3) proceeds as it does in the surrounding area of the n-butane vertex. This reactive azeotrope point has been reported previously by Ung and Doherty[6] and Taylor et al.[66] using the EQ model approach at different pressures. The effect of including the non-equilibrium condition is evident at each curve, the NEQ curves that originate in the azeotrope point are completely displaced with respect to the EQ curves. Also, the composition lines starting in the n-butane – *i*-butene vertex have different slopes increasing when the curves are in the vicinity of the reactive vertex.

Table 6-2. Reactive azeotrope point coordinates

	NEQ model	EQ model
X_1	0.035091	0.008008
X_2	0.010644	0.002103
X_3	0.954265	0.989889
T(K)	357.65	357.55

6.5 Case of Study 2: TAME

Another process to draw the equilibrium and nonequilibrium curve maps in the limit of reaction equilibrium is the TAME synthesis. The reactions and kinetic expression appears in section 4.4. In addition the thermodynamic equilibrium constants are taken from Oost et al.[48]

For this study we have to consider two simultaneous reactions, The TAME synthesis from the isoamylenes (equation (4.17)) and the isomerisation (equation (4.16)),

$$2A_1 + A_2 + A_3 \rightleftharpoons 2A_4 \tag{6.48}$$

$$A_2 \rightleftharpoons A_3 \tag{6.49}$$

where methanol is component A_1, 2-methyl-1-butene (2MB1) is component A_2, 2-methyl-2-butene (2MB2) is component A_3, TAME is component A_4, and with the presence of n-pentane (A_5) as inert. The degrees of freedom for this reactive system is two (*c*-*R*-1=5-2-1=2), and the reactive composition curve map can be represented in a two dimensional transformed composition coordinates. Two reference components must be chosen, A_2 and A_3 are suitable choices since $[\nu_{\text{Ref}}]$ is nonsingular, then

$$(x_{\text{Ref}}) = \begin{pmatrix} x_2 \\ x_3 \end{pmatrix}$$

$$[\nu_{\text{Ref}}] = \begin{bmatrix} -1 & -1 \\ -1 & 1 \end{bmatrix}$$

and

$$(\nu_T) = (-2, 0)$$

The transformed composition variables are

$$X_1 = \frac{x_1 - x_3 - x_2}{1 - x_3 - x_2} \tag{6.50}$$

$$X_4 = \frac{x_4 + x_2 + x_3}{1 - x_3 - x_2} \tag{6.51}$$

$$X_5 = \frac{x_5}{1 - x_3 - x_2} \tag{6.52}$$

Only two transformed variables are independent due to equation (6.40) and X_1 and X_5 are chosen as independent variables. For this set of coordinates the composition space is contained by a trapezoid. The equilibrium and non-equilibrium residue composition maps for TAME synthesis at P= 2.5 atm are shown in Figure 6-5. The two types or residue composition maps

localize one non-reactive azeotrope at T=330.089 K in the methanol – n-pentane side that remains after the reaction. We deduce from this residue composition map that there are no reactive azeotropes, but steady state solutions of residue composition maps are necessary to be sure that there are not distillation boundaries in the mixture.

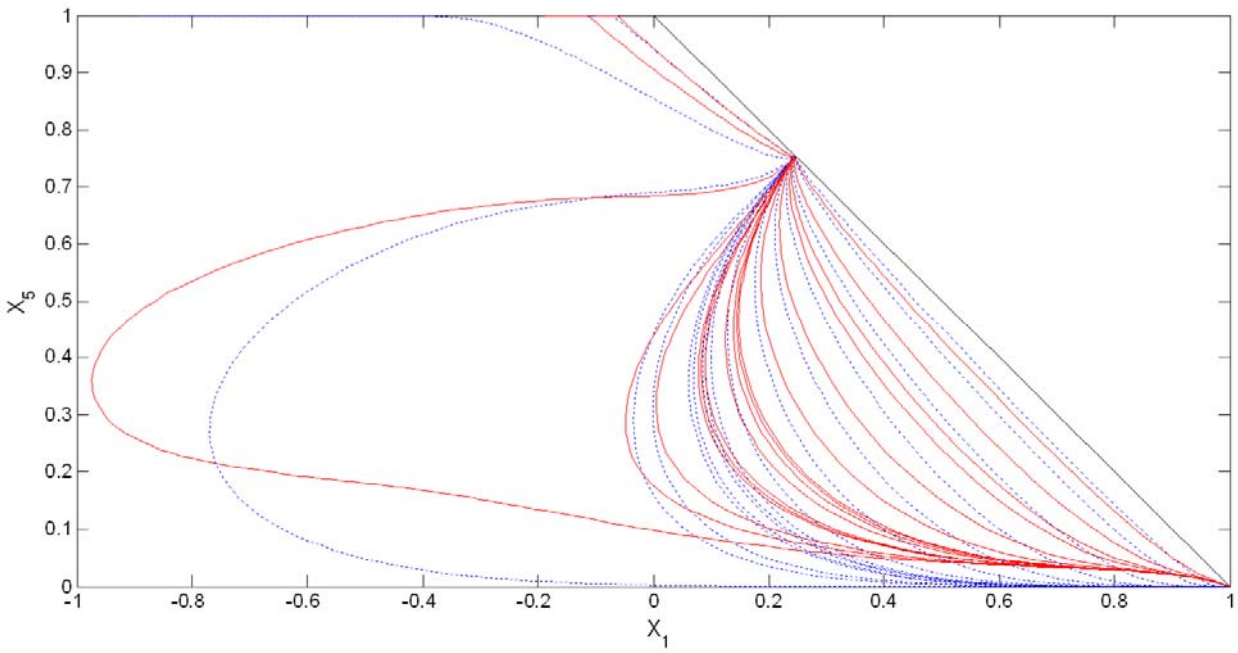

Figure 6-5. Non-equilibrium reactive composition curves (solid red lines) and equilibrium reactive composition curves (dashed blue lines) in transformed composition variables for TAME synthesis

6.6 Conclusions

We have derived a new expression to relate liquid and vapor bulk composition for reactive separation processes at total reflux condition in terms of the mass transfer coefficients and design aspects to draw non-equilibrium composition maps. In this work it was also demonstrated that for reactive azeotrope points in the MTBE synthesis the equilibrium and non-equilibrium composition maps are not the same, contrary to non-reactive separation systems where all stationary points are similar within the two models. For TAME synthesis,

the nonequilibrium and equilibrium reactive composition curve maps in the limit of reaction equilibrium were reported and the two models localized one non-reactive azeotrope. But steady state solutions of residue composition maps are necessary to be sure that there are none distillation boundaries in the mixture.

Conclusions

The Damköhler number is an important parameter to investigate the MSS phenomena in modeling reactive separation processes because it facilitates the simultaneously study of the reaction and physical separation processes, that at a critical Da values it produces multiplicities.

The Rachford-Rice procedure used to solve non-reactive flash isothermal isobaric flash processes can be extended to reactive systems. While isothermal CSTR problems and isothermal non-reactive flash problems do not exhibit Hopf bifurcations, isothermal reactive flash process problems involving MTBE and TAME mixtures do exhibit Hopf bifurcations.

The imposition of the mass-transfer equations on the reactive flash problem leads to the formation of limit points in the case of the TAME mixture and isolas with intersecting branches in the case of the MTBE problem.

It was also demonstrated that for reactive azeotrope points in the MTBE synthesis the equilibrium and non-equilibrium composition maps are not the same, contrary to non-reactive separation systems where all stationary points are similar within the two models.

For TAME synthesis, the nonequilibrium and equilibrium reactive composition curve maps in the limit of reaction equilibrium were reported and the two models localized one non-reactive azeotrope. To confirm that there are not distillation boundaries in the mixture, steady state solutions of residue composition maps are required.

Future work on applying the continuation analysis to find singular points in multistage EQ and NEQ reactive distillation must be considered including packed columns. In the design and synthesis area, kinetic effects on nonequilibrium composition curve maps must be implemented.

Appendix A. Physical Properties

The diffusion coefficients in the gas mixture are estimated using the Fuller–Schettler-Giddings method[60]. The equation of the diffusivity is

$$D = CT^{1.75} \frac{\sqrt{\dfrac{M_1 + M_2}{M_1 M_2}}}{P\left\{\sqrt[3]{V_1} + \sqrt[3]{V_2}\right\}^2} \tag{A.1}$$

where C = 1.013e-02, T is in K, P in Pa and M in kg/mol. The units of D is in m^2/s V is the molecular diffusion volume calculated by using the procedures in Taylor and Krishna [60].

The binary Fick diffusivity for each pair of components in the liquid mixture is from the Maxwell-Stefan diffusion coefficients

$$D_{ij} = \mathcal{D}_{ij} \Gamma_{ij} \tag{A.2}$$

$$\mathcal{D}_{ij} = \left(\mathcal{D}_{ij}^{\circ}\right)^{(1+x_j - x_i)/2} \left(\mathcal{D}_{ji}^{\circ}\right)^{(1+x_i - x_j)/2} \tag{A.3}$$

Here $\mathcal{D}_{ij}^{0}$ is the diffusion coefficient at infinite dilution, this is calculated using any correlation from table 4.2 in Taylor and Krishna[60]. The thermodynamic factor Γ,

$$\Gamma_{ij} = \delta_{ij} + x_i \left.\frac{\partial \ln \gamma_i}{\partial x_j}\right|_{T,P} \qquad \delta_{ij} = \begin{cases} 1, & i = j \\ 0, & i \neq j \end{cases} \tag{A.4}$$

The density of liquid mixture is estimated using the Hankinson-Brobst-Thomson (HBT) technique[70]. The density of the gas mixture and the residual properties (ΔH_{Res}, ΔCp_{Res}) are estimated using the Lee and Kesler correlation[71]. The surface tension (σ) is estimated using the Macleod-Sugden correlation[70]. The viscosity (μ) of gas mixture is calculated by Lucas

Method[70]. The vapor pressure $\left(P_i^{\text{sat}}\right)$, liquid and vapor enthalpy (ΔH), and the heat capacity at constant pressure (C_P) are estimated using the correlation parameters from the Chemical Properties Handbook[72]. The liquid thermal conductivity (λ) of liquid mixture is calculated using the Li and Latini Methods[70].

The mass transfer coefficients are obtained using the AIChE method[57] with the modification of Bennett et al.[58], as follows,

$$\left[\kappa^V\right] = \left[R^V\right]^{-1} \tag{A.5}$$

$$\left[\kappa^L\right] = \left[R^L\right]^{-1}\left[\Gamma\right] \tag{A.6}$$

$$\left[R^V\right] = \begin{cases} R_{ii}^V = \dfrac{y_i}{\kappa_{in}^V} + \displaystyle\sum_{\substack{k=1\\k\neq i}}^{n} \dfrac{y_k}{\kappa_{ik}^V} \\ R_{ij}^V = -y_i\left(\dfrac{1}{\kappa_{ij}^V} - \dfrac{1}{\kappa_{in}^V}\right) \end{cases} \tag{A.7}$$

$$\left[R^L\right] = \begin{cases} R_{ii}^L = \dfrac{x_i}{\kappa_{in}^L} + \displaystyle\sum_{\substack{k=1\\k\neq i}}^{n} \dfrac{x_k}{\kappa_{ik}^L} \\ R_{ij}^L = -x_i\left(\dfrac{1}{\kappa_{ij}^L} - \dfrac{1}{\kappa_{in}^L}\right) \end{cases} \tag{A.8}$$

$$\kappa_{ij}^V = \frac{\aleph_{ij}^V u_s}{a h_f} \tag{A.9}$$

$$\kappa_{ij}^L = \frac{\aleph_{ij}^L \left(Q_L / W\right)}{a h_f Z} \tag{A.10}$$

$$Q_V = \frac{V}{c_t^V} \tag{A.11}$$

$$Q_L = \frac{L}{c_t^L} \tag{A.12}$$

$$\aleph_{ij}^V = \left(0.776 + 4.567h_w - 0.238F_s + 104\left(\frac{Q_L}{W}\right)\right)\mathrm{Scv}_{ij}^{-0.5} \tag{A.13}$$

$$\mathrm{Scv}_{ij} = \frac{\mu_i^V}{\rho_t^V D_{ij}^V} \tag{A.14}$$

$$\aleph_{ij}^L = 19700\left(D_{ij}^L\right)^{0.5}\left(0.4F_s + 0.17\right)t_L \tag{A.15}$$

$$t_L = \frac{h_L ZW}{Q_L} \tag{A.16}$$

The liquid heat transfer coefficient is obtained using the penetration model[60] and the vapor heat transfer coefficient is calculated using the Chilton-Colburn analogy[60], as follows

$$\mathbf{h}^L = 2\rho_t C_p \sqrt{\frac{\lambda}{\rho_t C_p \pi t_e}} \tag{A.17}$$

Where t_e is the exposure time. It is better to express the heat transfer coefficient as function of dimensional numbers. Lewis number $\mathrm{Le} = \frac{\mathrm{Sc}}{\mathrm{Pr}}$ were Sc is the Schmidt number $\mathrm{Sc} = \frac{\mu}{\rho_t D}$ and Pr is the Prandtl number $\mathrm{Pr} = \frac{C_p \mu}{\lambda}$. Replacing Sc and Pr numbers in Le, $\mathrm{Le} = \frac{\lambda}{\rho_t D C_p}$, and substituting the new expression for Le in (A.17) we get,:

$$\mathbf{h}^L = 2\rho_t C_p \sqrt{\mathrm{Le}\frac{D}{\pi t_e}} \tag{A.18}$$

The average mass transfer coefficient can be defined as $\bar{\kappa} = 2\sqrt{\frac{D}{\pi t_e}}$, substituting $\bar{\kappa}$ in (A.18):

$$\mathbf{h}^L = \bar{\kappa}\rho_t C_p{}^L \,\mathrm{Le}^{1/2} \tag{A.19}$$

The vapor heat transfer coefficient is obtained using the Chilton-Colburn analogy,

$$j_D = j_H \tag{A.20}$$

$$j_D = \mathrm{St}\ \mathrm{Sc}^{2/3} \tag{A.21}$$

$$j_H = \mathrm{St}_H\ \mathrm{Pr}^{2/3} \tag{A.22}$$

St is the Stanton number $\mathrm{St} = \frac{\overline{\kappa}}{\overline{u}}$, where $\overline{u}$ is mean velocity for flow. St_H is the Stanton number for heat transfer $\mathrm{St}_H = \frac{\mathbf{h}^V}{\rho_t C_p \overline{u}}$

Substituting (A.21) and (A.22) in (A.20):

$$\mathrm{St}\ \mathrm{Sc}^{2/3} = \mathrm{St}_H\ \mathrm{Pr}^{2/3} \tag{A.23}$$

$$\mathrm{St}_H = \mathrm{St}\left(\frac{\mathrm{Sc}}{\mathrm{Pr}}\right)^{2/3} \tag{A.24}$$

$$\frac{\mathbf{h}^V}{\rho_t C_p \overline{u}} = \mathrm{St}\left(\frac{\mathrm{Sc}}{\mathrm{Pr}}\right)^{2/3} \tag{A.25}$$

$$\mathbf{h}^V = \mathrm{St}\,\overline{u}\rho_t C_p\left(\frac{\mathrm{Sc}}{\mathrm{Pr}}\right)^{2/3} \tag{A.26}$$

$$\mathbf{h}^V = \overline{\kappa}\rho_t C_p{}^V\ \mathrm{Le}^{2/3} \tag{A.27}$$

The calculation of the enthalpy of a component is calculated taking 295 K and 1 atm as elemental reference state. A schematic representation is showed in the Figure A-1.

Now, the calculation of the enthalpy of the liquid and vapor mixture are:

$$H^L_{\mathrm{mix}} = \sum_{i=1}^{c} x_i H_i^L + \Delta H^L_{\mathrm{mix}} \tag{A.28}$$

$$H^V_{\mathrm{mix}} = \sum_{i=1}^{c} y_i H_i^V + \Delta H^V_{\mathrm{mix}} \tag{A.29}$$

where H_i is the enthalpy of component in the respective phase, and ΔH_{mix} is the mixing enthalpy, in this work ΔH_{mix} is not considered.

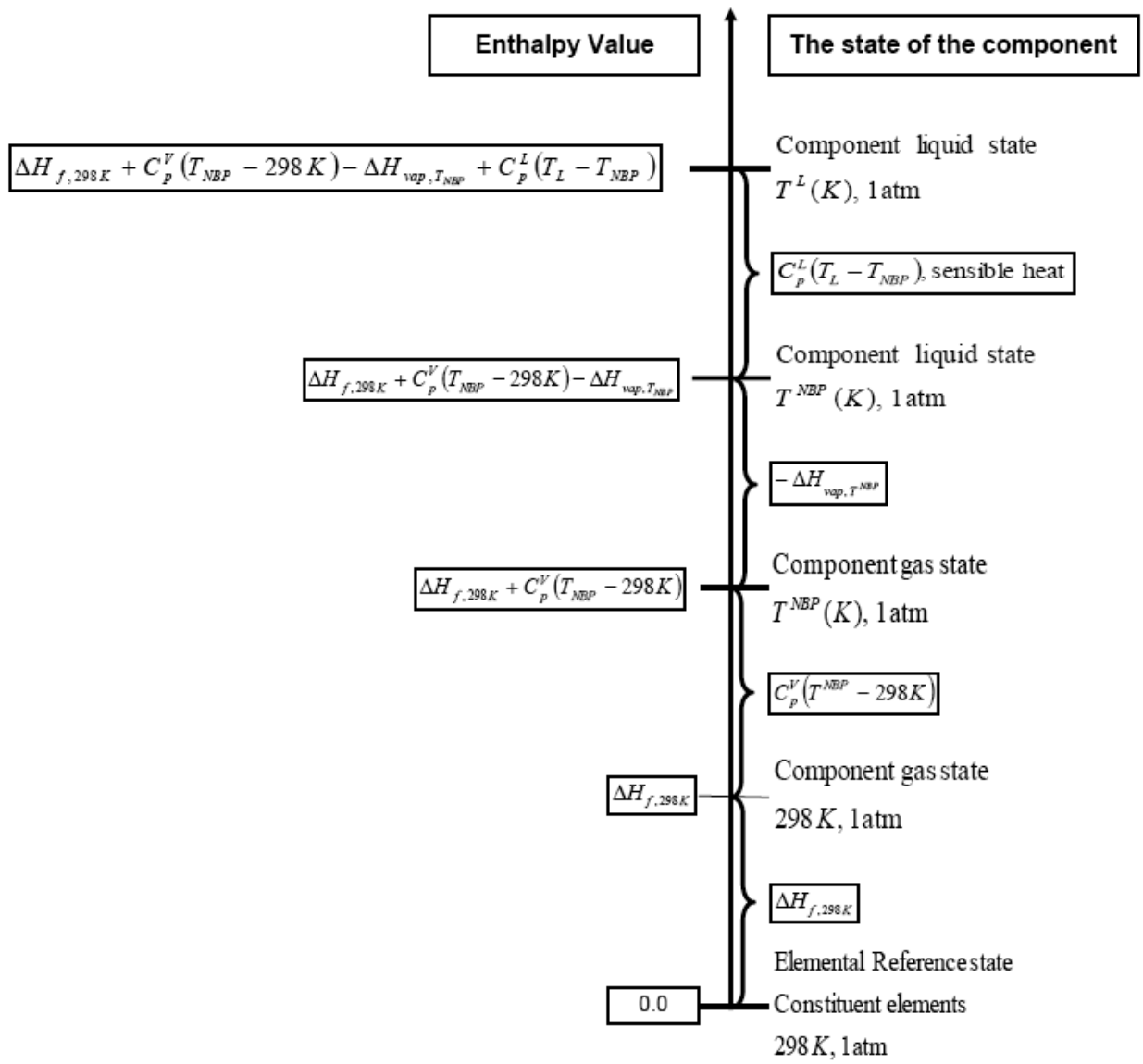

Figure A-1. Calculation of the enthalpy of a component.

Appendix B. Tray Design Procedure

The tray design procedure is briefly described in this appendix. We follow the procedure described in Locket[68] and Kooijman[73]. Fixing the tray spacing T_s , the number of passes N_{passes}, the weir height h_w, the fractional perforated tray area ϕ, the downcomer clearance h_c and the hole diameter d_h, the tray thickness t_t will be given by $t_t = 0.43 d_h$.

The volumetric liquid flow Q_L is known and this enables us to calculate the downcomer area A_d and u_d the liquid velocity in downcomer on vapor free basis using the relationship

$$u_d = \frac{Q_L}{A_d} = 0.0081\left(T_s\right)^{0.5}\left(\rho_t^L - \rho_t^V\right)^{0.5} \tag{B.1}$$

FP the flow parameter is then calculated as

$$FP = \left(M_L / M_V\right)\left(\rho_t^V / \rho_t^L\right)^{0.5} \tag{B.2}$$

where if *FP* is found to be less than 0.1it was rounded to 0.1. The capacity factor based on the tray spacing (*CF''*) is given by

$$CF'' = \left(0.0744 T_s + 0.0117\right)\left(\log_{10}\left(FP^{-1}\right)\right) + 0.0304 T_s + 0.0153 \tag{B.3}$$

while the capacity factor *CF*' based on the net area for the liquid disengagement above the tray (A_n) is defined by the expression

$$CF' = CF''\left(\frac{\sigma}{0.02}\right)^{0.2}\left(\frac{\phi}{0.1}\right)^{0.44} \tag{B.4}$$

The expression for *CF*' in Locket[68] is used to obtain $u_s^{'}$

$$CF' = u_s' \left(\frac{\rho_t^V}{\rho_t^L - \rho_t^V} \right)^{0.5} \tag{B.5}$$

and the expression $u_s' = \frac{Q_V}{A_n}$ is used to calculate A_n

$$A_b = A_n - A_d \tag{B.6}$$

the total area of the tray is given by $A_{\text{total}} = A_b + 2A_d$

The total diameter (D_{total}) is estimated by

$$D_{\text{total}} = \left(\frac{4A_{\text{total}}}{\pi} \right)^{0.5} \tag{B.7}$$

the liquid flow path length (Z) and the weir length (W) are determined as follows.

defining $x_1 = (\frac{W}{D_{\text{total}}}) * 100$, $y_1 = \frac{A_d}{A_{\text{total}}} * 100$ and $y_2 = \frac{w_d}{D_{\text{total}}} * 100$ we use the expressions from Figure 8.69 in Ludwig[74],

$$x_1 = -0.0004 y_1^4 + 0.026 y_1^3 - 0.6345 y_1^2 + 8.4998 y_1 + 29.408 \tag{B.8}$$

$$y_2 = 9 * 10^{-5} x_1^3 - 0.0113 x_1^2 + 0.7328 x_1 - 12.991 \tag{B.9}$$

to obtain W, w_d and Z by equations:

$$W = x_1 * \mathrm{D}_{\text{total}} / 100 \tag{B.10}$$

$$w_d = y_2 * \mathrm{D}_{\text{total}} / 100 \tag{B.11}$$

$$Z = \mathrm{D}_{\text{total}} - 2 * w_d \tag{B.12}$$

The weir load (Q_L / W) must be less or equal that maximum weir load $(Q_L / W)_{\max}$, and this maximum value is estimated using the correlation in locket[68]

$$(Q_L / W)_{\max} = 0.087 T_s - 0.0204 \tag{B.13}$$

If the weir load is more that the maximum value, the number of passes is incremented.

With the superficial vapor velocity $u_S = \frac{Q_V}{A_b}$, the clear liquid height h_L is computed using expressions from Bennett et al.[58]:

$$h_L = \alpha_e \left\{ h_w + C\left(Q_L / \left(W\alpha_e\right)\right)^{0.67} \right\} \tag{B.14}$$

where

$$\alpha_e = \exp\left\{ -12.55\left(u_s \left\{ \rho_t^V / \left(\rho_t^L - \rho_t^V\right)\right\}^{0.5}\right)^{0.91} \right\} \tag{B.15}$$

and

$$C = 0.5 + 0.438\exp\left(-137.8h_w\right) \tag{B.16}$$

To avoid weeping it is crucial to establish a suitable free area ratio such that the Froude number Fr_h based on u_h which should be less or equal to 2/3. It is necessary to keep ϕ in the range ($0.05 < \phi < 0.2$). The Fr_h is obtained with the expression

$$\mathrm{Fr}_h = u_h \left(\frac{\rho_t^V}{gh_L\left(\rho_t^L - \rho_t^V\right)} \right)^{0.5} \tag{B.17}$$

where

$$u_h = \frac{Q_V}{A_h} \tag{B.18}$$

We start with

$$\phi = \frac{A_h}{A_b} \tag{B.19}$$

and obtain A_h. This is used to find u_h which is used to obtain the Froude number Fr_h. If the Froude number Fr_h is not suitable a new value of ϕ is chosen and the procedure is repeated.

The parameter ah_f (a is the interfacial area per unit volume of froth and h_f is the froth height) is calculated using the Zuiderweg method[59], which takes into account the nature of the flow regime (spray or mixed froth emulsion). For spray regime:

$$ah_f = \frac{40}{\phi^{0.3}}\left(\frac{u_s^{\,2}\rho_t^V h_L^{\,*} FP}{\sigma}\right)^{0.37} \tag{B.20}$$

for mixed froth emulsion flow regime:

$$ah_f = \frac{43}{\phi^{0.3}}\left(\frac{u_s^{\,2}\rho_t^V h_L^{\,*} FP}{\sigma}\right)^{0.53} \tag{B.21}$$

the transition from spray to froth emulsion flow occurs if $FP > 3.0bh_L^{\,*}$, where b is the weir length per unit bubbling area

$$b = \frac{W}{A_b} \tag{B.22}$$

σ is the surface tension and $h_L^{\,*}$ is the clear liquid height, give by the Zuiderweg correlation[59]

$$h_L^{\,*} = 0.6h_w^{\,0.5}\left(\frac{pFP}{b}\right)^{0.25} \tag{B.23}$$

p is the hole pitch, for 60° triangular pitch perforations, and is calculated as

$$p = \left[\frac{\pi}{2\sqrt{3}}\frac{d_h^{\,2}}{\varphi}\right]^{0.5} \tag{B.24}$$

The liquid holdup fraction (α) is also calculated based on the regime type, as shown by Colwell[75].

For the froth regime we have

$$\alpha = \frac{1}{\eta + 1} \tag{B.25}$$

$$\eta = 12.6\left(\mathrm{Fr}'\right)^{0.4}\phi^{-0.25} \tag{B.26}$$

$$\mathrm{Fr}' = \frac{u_s^{\ 2}}{gh_L}\frac{\rho_t^V}{\rho_t^L - \rho_t^V} \tag{B.27}$$

while the correlation given by Stichlmair[68] is used for the spray regime. This correlation is

$$\alpha = 1 - \left(\frac{F_s}{F_{s,\max}}\right) \tag{B.28}$$

$$F_s = u_s\left(\rho_t^V\right)^{0.5} \tag{B.29}$$

$$F_{s,\max} = 2.5\left(\phi^2\sigma\left(\rho_t^L - \rho_t^V\right)g\right)^{0.25} \tag{B.30}$$

where g is the acceleration due to gravity and F_s is the superficial flow factor.

The froth height h_f is given by

$$h_f = \frac{h_L}{\alpha} \tag{B.31}$$

the liquid and vapor holdups and the net interfacial area are calculated using the equations

$$\varepsilon^L = A_b h_L c_t^L \tag{B.32}$$

$$\varepsilon^V = \frac{1-\alpha}{\alpha}\varepsilon^L \tag{B.33}$$

and

$$a_{\mathrm{net}} = a h_f A_b \tag{B.34}$$

To determine the downcomer backup

$$h_{fd} = \frac{\left(h_{WT} + h_{cli} + h_{udc} + h_n\right)}{\overline{\alpha_d}} \tag{B.35}$$

$$h_{udc} = \frac{1}{2g}\left(\frac{Q_L}{Wh_L C_d}\right)^2 \tag{B.36}$$

$C_d = 0.54$ or 0.60

$$h_{cli} = h_i \tag{B.37}$$

From Figure 5.10 in Locket[68]:

$$x_2 = \rho_t^L - \rho_t^V \tag{B.38}$$

$$\overline{\alpha}_d = -5E-9x_2^{\ 3} + 5E-6x_2^{\ 2} - 0.0013x_2 + 0.4571 \tag{B.39}$$

$$200 \le x_2 \le 577, \text{ if } x_2 > 577, \text{ then } \overline{\alpha}_d = 0.6 \tag{B.40}$$

$$h_i = \left[\frac{2}{g}\left(\frac{Q_L}{W}\right)^2 \left(\frac{1}{h_L} - \frac{1}{h_c}\right) + \frac{2\alpha h_f^{\ 2}}{3} \right]^{0.5} \tag{B.41}$$

h_n is almost always neglected in calculating downcomer backup at the design stage because it acts conventionally and reduces backup[68].

The design condition for height of clear liquid in the downcomer for flooding is usually set a 0.6 to 0.8 of $T_s + h_W$

To determine the total tray pressure drop

$$h_{WT} = h_{DT} + h_L + h_R \tag{B.42}$$

$$h_{DT} = \frac{\xi \rho_t^V u_h^{\ 2}}{2g\rho_t^L} \tag{B.43}$$

$$\xi = C_d^{\ -2} \tag{B.44}$$

$$h_R = \left(\frac{6}{1.27\rho_t^L}\right)\left(\frac{\sigma}{g}\right)^{2/3}\left(\frac{\rho_t^L - \rho_t^V}{d_h}\right)^{0.33} \tag{B.45}$$

Nomenclature

a_{net}	net interfacial area, m^2
A_b	bubbling area of the tray, m^2
A_d	downcomer area, m^2
A_h	total area of the holes, m^2
A_n	net area for liquid disengagement above tray, m^2
A_{total}	total cross sectional area, m^2
C_d	discharge coefficient
C_p	Heat capacity, kJ kg^{-1} K^{-1}
c_t	total concentration, kmol m^{-3}
CF'	capacity factor based on A_n
d	some characteristic dimension of the equipment, m
d_h	hole diameter, m
D	Fick diffusivity, m^2 s^{-1}
$\mathcal{D}$	Maxwell-Estefan diffusivity, m^2 s^{-1}
D_{total}	column diameter, m
$\overline{D}$	average Fick diffusivity, m^2 s^{-1}
Fr_h	Froude number
F_s	supercritical F factor

FF	flood factor or fractional approach to flooding
g	acceleration due to gravity, 9.80 m s^{-2}
h	heat transfer coefficient, W m^{-2} K^{-1}
h_{cli}	clear liquid height at liquid entry, m
h_f	froth height, m
h_{fd}	downcomer backup, m
h_i	depth of liquid at liquid entry, m
h_n	pressure increase across the nappe, m
h_{udc}	pressure drop under the downcomer, m
h_w	exit weir height, m
h_{DT}	dry tray pressure drop, m
h_L	clear liquid height, m
h_R	residual pressure drop, m
h_{WT}	wet or total tray pressure drop, m
H	molar enthalpy, J $kmol^{-1}$
$\overline{H}$	partial molar enthalpy, J $kmol^{-1}$
M_L	liquid flow rate, kg s^{-1}
M_V	vapor flow rate, kg s^{-1}
p	hole pitch, m
P_r	Prandtl number
$(Q_L / W)_{max}$	maximum weir load

Q_L	volumetric liquid flow rate, $m^3\ s^{-1}$
Q_V	volumetric vapor flow rate, $m^3\ s^{-1}$
$\mathbb{R}$	gas constant, J $kmol^{-1}\ K^{-1}$
Re	Reynolds number
St_H	Stanton number
t_t	tray thickness, m
T_s	tray spacing, m
u	velocity, m s^{-1}
u_d	liquid velocity in downcomer on vapor-free basis, m s^{-1}
u_h	vapor velocity through holes, m s^{-1}
u_s	supercritical vapor velocity based on the bubbling area of the tray, m s^{-1}
W	weir length, m
w_d	downcomer width, m
Z	liquid flow path length, m

Greek

α	liquid holdup fraction
$\overline{\alpha}_d$	mean liquid volume fraction in the downcomer
ε	reaction holdup, kmol
ε_g	gas holdup fraction
$\overline{\kappa}$	average mass transfer coefficient, m s^{-1}

μ	chemical potential, J kmol^{-1}
μ	viscosity, N s m^{-2}
λ	thermal conductivity, W m^{-1} K^{-1}
$\nu_{i,m}$	stoichiometric coefficient of component *i* in reaction *m*
ξ	orifice coefficient
η	distance along diffusion path, dimensionless
σ	surface tension, N m^{-1}
φ	fractional perforated tray area
$\aleph$	number of transfer units

Subscripts

i	component index
I	referring to interface
j	stage index
k	index
m	reaction index

Superscripts

F	referring to feed stream
I	referring to interface
L	referring to liquid phase
V	referring to vapor phase

References

1. Higler, A. P.; Taylor, R.; Krishna, R., Nonequilibrium modelling of reactive distillation: Multiple steady states in MTBE synthesis. *Chemical Engineering Science* **1999,** 54, (10), 1389-1395.

2. Sundmacher, K.; Uhde, G.; Hoffmann, U., Multiple reactions in catalytic distillation processes for the production of the fuel oxygenates MTBE and TAME: analysis by rigorous model and experimental validation. *Chemical Engineering Science* **1999,** 54, (13-14), 2839-2847.

3. Higler, A.; Krishna, R.; Taylor, R., Nonequilibrium modeling of reactive distillation: a dusty fluid model for heterogeneously catalyzed processes. *Industrial and Engineering Chemistry Research* **2000,** 39, (6), 1596-1607.

4. Chen, F.; Huss, R. S.; Doherty, M. F.; Malone, M. F., Multiple steady states in reactive distillation: Kinetic effects. *Computers and Chemical Engineering* **2002,** 26, (1), 81-93.

5. Barbosa, D.; Doherty, M. F., The simple distillation of homogeneous reactive mixtures. *Chemical Engineering Science* **1988,** 43, (3), 541-550.

6. Ung, S.; Doherty, M. F., Calculation of residue curve maps for mixtures with multiple equilibrium chemical reactions. *Ind. Eng. Chem. Res.* **1995,** 34, (10), 3195-3202.

7. Castillo, F. J. L.; Towler, G. P., Influence of multicomponent mass transfer on homogeneous azeotropic distillation. *Chemical Engineering Science* **1998,** 53, (5), 963-976.

8. Taylor, R.; Baur, R.; Krishna, R., Influence of mass transfer in distillation: Residue curves and total reflux. *AIChE Journal* **2004,** 50, (12), 3134-3148.

9. Sridhar, L. N.; Maldonado, C.; Garcia, A.; Irizzarry, J., Heterogeneous nonequilibrium mole fraction curve maps. *Ind. Eng. Chem. Res.* **2005,** 44, (8), 2845-2847.

10. Sridhar, L. N.; Maldonado, C.; Garcia, A. M., Design and analysis of nonequilibrium separation processes. *AIChE Journal* **2002,** 48, (6), 1179-1191.

11. Chen, F.; Huss, R. S.; Malone, M. F.; Doherty, M. F., Simulation of kinetic effects in reactive distillation. *Computers & Chemical Engineering* **2000,** 24, (11), 2457-2472.

12. The MathWorks, I. Optimization Toolbox for use with MATLAB user's guide. www.mathworks.com

13. Okasinski, M. J.; Doherty, M. F., Design Method for Kinetically Controlled, Staged Reactive Distillation Columns. *Ind. Eng. Chem. Res.* **1998,** 37, (7), 2821-2834.

14. Sridhar, L. N.; Lucia, A., Analysis and algorithms for multistage separation processes. *Ind. Eng. Chem. Res.* **1989,** 28, (6), 793-803.

15. Sridhar, L. N., Multistage standard specification. *AIChE Journal* **1997,** 43, (5), 1369-1371.

16. Sridhar, L. N., Analysis of two-stage heterogeneous separation processes. *AIChE Journal* **1996,** 42, (10), 2761-2764.

17. Sridhar, L. N.; Maldonado, C.; Garcia, A.; de Frias, A., Analysis of single-stage nonequilibrium separation process problems. *AIChE Journal* **2000,** 46, (11), 2237-2244.

18. Pisarenko, Y. A.; Epifanova, O. A.; Serafimov, L. A., Conditions for a steady state in a reactive distillation operation. *Theoretical Foundations of Chemical Engineering* **1988,** 22, 31–34

19. Nijhuis, S. A.; Kerkhof, F. P. J. M.; Mak, A. N. S., Multiple steady states during reactive distillation of methyl tert-butyl ether. *Industrial & Engineering Chemistry Research* **1993,** 32, (11), 2767-2774.

20. Hauan, S.; Hertzberg, T.; Lien, K. M., Multiplicity in reactive distillation of MTBE. *Computers & Chemical Engineering* **1997,** 21, (10), 1117-1124.

21. Hauan, S.; Schrans, S. M.; Lien, K. M., Dynamic evidence of the multiplicity mechanism in methyl tert-butyl ether reactive distillation. *Industrial & Engineering Chemistry Research* **1997,** 36, (9), 3995-3998.

22. Mohl, K.-D.; Kienle, A.; Gilles, E.-D., Multiple steady states in a reactive distillation column for the production of the fuel ether TAME I. Theoretical analysis. *Chemical Engineering & Technology* **1998,** 21, (2), 133-136.

23. Guttinger, T. E.; Morari, M., Predicting multiple steady states in equilibrium reactive distillation. 1. Analysis of nonhybrid systems. *Industrial and Engineering Chemistry Research* **1999,** 38, (4), 1633-1648.

24. Guttinger, T. E.; Morari, M., Predicting multiple steady states in equilibrium reactive distillation. 2. Analysis of hybrid systems. *Industrial and Engineering Chemistry Research* **1999,** 38, (4), 1649-1665.

25. Jacobs, R.; Krishna, R., Multiple solutions in reactive distillation for methyl tert-butyl ether synthesis. *Industrial & Engineering Chemistry Research* **1993,** 32, (8), 1706-1709.

26. Mohl, K.-D.; Kienle, A.; Gilles, E.-D.; Rapmund, P.; Sundmacher, K.; Hoffmann, U., Steady-state multiplicities in reactive distillation columns for the production of fuel ethers MTBE and TAME: theoretical analysis and experimental verification. *Chemical Engineering Science* **1999,** 54, (8), 1029-1043.

27. Mueller, D.; Marquardt, W., Experimental verification of multiple steady states in heterogeneous azeotropic distillation. *Industrial & Engineering Chemistry Research* **1997,** 36, (12), 5410-5418.

28. Rapmund, P.; Sundmacher, K.; Hoffmann, U., Multiple steady states in a reactive distillation column for the production of the fuel ether TAME Part II: Experimental validation. *Chemical Engineering & Technology* **1998,** 21, (2), 136-139.

29. Rehfinger, A.; Hoffmann, U., Kinetics of methyl tertiary butyl ether liquid phase synthesis catalyzed by ion exchange resin--I. Intrinsic rate expression in liquid phase activities. *Chemical Engineering Science* **1990,** 45, (6), 1605-1617.

30. Venimadhavan, G.; Buzad, G.; Doherty, M. F.; Malone, M. F., Effect of kinetics on residue curve maps for reactive distillation. *AIChE Journal* **1994,** 40, (11), 1814-1824.

31. Barbosa, D. Distillation of Reactive Mixtures. University of Massachusetts, Amherst, MA, USA, 1987.

32. Ung, S.; Doherty, M. F., Vapor-liquid phase equilibrium in systems with multiple chemical reactions. *Chemical Engineering Science* **1995,** 50, (1), 23-48.

33. Dhooge, A.; Govaerts, W.; Kuznetsov, Y. A.; Mestrom, W.; Riet, A. M. CL_MATCONT: A continuation toolbox in MATLAB.

34. Seydel, R., *Practical Bifurcation and Stability Analysis: From Equilibrium to Chaos* 2ed.; Springer Verlag: New York, NY, USA, 1994; p 407.

35. GOVAERTS, W.; Belgium, F. W. O.; KUZNETSOV, Y. A.; CWI, A.; SIJNAVE, B., Implementation of Hopf and Double-Hopf Continuation Using Bordering Methods. *ACM Transactions on Mathematical Software* **1998,** 24, (4), 418-436.

36. Taylor, R.; Krishna, R., Modelling reactive distillation. *Chemical Engineering Science* **2000,** 55, (22), 5183-5229.

37. Bravo, J. L.; Pyhalahti, A.; Jarvelin, H., Investigations in a catalytic distillation pilot plant. Vapor/liquid equilibrium kinetics, and mass-transfer issues. *Ind. Eng. Chem. Res.* **1993,** 32, (10), 2220-2225.

38. Hauan, S.; Hertzberg, T.; Lien, K. M., Multiplicity in reactive distillation of MTBE. *Computers & Chemical Engineering* **1995,** 19, (Suppl), 327-332.
39. Hauan, S.; Schrans, S. M.; Lien, K. M., Dynamic Evidence of the Multiplicity Mechanism in Methyl tert-Butyl Ether Reactive Distillation. *Ind. Eng. Chem. Res.* **1997,** 36, (9), 3995-3998.

40. Sneesby, M. G.; Tade, M. O.; Smith, T. N., Steady-state transitions in the reactive distillation of MTBE. *Computers & Chemical Engineering* **1998,** 22, (7-8), 879-892.

41. Sneesby, M. G.; Tade, M. O.; Smith, T. N., Multiplicity and pseudo-multiplicity in MTBE and ETBE reactive distillation. *Chemical Engineering Research & Design, Transactions of the Institute of Chemical Engineers, Part A* **1998,** 76, (A4), 525-531.

42. Eldarsi, H. S.; Douglas, P. L., Methyl-tert-butyl-ether catalytic distillation column, Part I: Multiple steady states. *Chemical Engineering Research & Design, Transactions of the Institute of Chemical Engineers, Part A* **1998,** 76, (A4), 509-516.

43. Rodriguez, I. E.; Zheng, A.; Malone, M. F., Parametric dependence of solution multiplicity in reactive flashes. *Chemical Engineering Science* **2004,** 59, (7), 1589-1600.

44. Rodríguez, I. E.; Zheng, A.; Malone, M. F., The stability of a reactive flash. *Chemical Engineering Science* **2001,** 56, (16), 4737-4745.

45. Lucia, A., Uniqueness of Solutions to Single-Stage Isobaric Flash Processes Involving Homogeneous Mixtures. *AIChE Journal* **1986,** 32, (11), 1761-1770.

46. Doherty, M. F.; Malone, M. F., *Conceptual Design of Distillation Systems*. McGraw-Hill: New York, NY USA, 2001; p 568.

47. Oost, C.; Hoffmann, U., Synthesis of tertiary amyl methyl ether (TAME): microkinetics of the reactions. *Chemical Engineering Science* **1996,** 51, (3), 329-340.

48. Oost, C.; Sundmacher, K.; Hoffmann, U., Synthesis of tertiary amyl methyl ether (TAME): equilibrium of the multiple reactions. *Chemical Engineering & Technology* **1995,** 18, (2), 110-117.

49. Rihko, L. K.; Krause, O. I., Kinetics of heterogeneously catalyzed tert-amyl methyl ether reactions in the liquid phase. *Industrial & Engineering Chemistry Research* **1995,** 34, (4), 1172-1180.

50. Rihko, L. K.; Linnekoski, J. A.; Krause, A. O. I., Reaction equilibria in the synthesis of 2-methoxy-2-methylbutane and 2-ethoxy-2-methylbutane in the liquid phase. *Journal of Chemical and Engineering Data* **1994,** 39, (4), 700-704.

51. Gani, R.; Jepsen, T. S.; Perez-Cisneros, E. S., A generalized reactive separation unit model. Modelling and simulation aspects. *Computers & Chemical Engineering* **1998,** 22, (Supplement 1), S363-S370.

52. Ruiz, G.; Sridhar, L. N.; Rengaswamy, R., Isothermal Isobaric Reactive Flash Problem. *Ind. Eng. Chem. Res.* **2006,** 45, (19), 6548-6554.

53. Baur, R.; Higler, A. P.; Taylor, R.; Krishna, R., Comparison of equilibrium stage and nonequilibrium stage models for reactive distillation. *Chemical Engineering Journal* **2000,** 76, (1), 33-47.

54. Baur, R.; Taylor, R.; Krishna, R. In *Influence of column hardware on the performance of reactive distillation columns*, Napoles, 2001; Elsevier Science B.V.: Napoles, 2001; pp 225-232.

55. Katariya, A. M.; Kamath, R. S.; Moudgalya, K. M.; Mahajani, S. M., Non-equilibrium stage modeling and non-linear dynamic effects in the synthesis of TAME by reactive distillation. *Computers & Chemical Engineering* In Press, Corrected Proof.

56. Baur, R.; Taylor, R.; Krishna, R., Bifurcation analysis for TAME synthesis in a reactive distillation column: Comparison of pseudo-homogeneous and heterogeneous reaction kinetics models. *Chemical Engineering and Processing* **2003,** 42, (3), 211-221.

57. Committee, T. D. S. o. t. R., *Bubble-tray Design Manual; prediction of fractionation efficiency*. American Institute of Chemical Engineers New York, NY, 1958; p 94.

58. Bennett, D. L.; Agrawal, R.; Cook, P. J., New Pressure Drop Correlation for Sieve Tray Distillation Columns. *AIChE Journal* **1983,** 29, (3), 434-442.

59. Zuiderweg, F. J., Sieve Trays - A View of the State of the Art. *Chemical Engineering Science* **1982,** 37, (10), 1441-1464.

60. Taylor, R.; Krishna, R., *Multicomponent Mass Transfer*. Wiley-Interscience New York, NY, 1993; p 616.

61. Ung, S.; Doherty, M. F., Theory of phase equilibria in multireaction systems. *Chemical Engineering Science* **1995,** 50, (20), 3201-3216.

62. Lucia, A.; Taylor, R., The geometry of separation boundaries: I. Basic theory and numerical support. *AIChE Journal* **2006,** 52, (2), 582-594.

63. Doherty, M. F.; Perkins, J. D., On the dynamics of distillation processes--III : The topological structure of ternary residue curve maps. *Chemical Engineering Science* **1979,** 34, (12), 1401-1414.

64. Pham, H. N.; Doherty, M. F., Design and synthesis of heterogeneous azeotropic distillations. I. Heterogeneous phase diagrams. *Chemical Engineering Science* **1990,** 45, (7), 1823-1836.

65. Van Dongen, D. B.; Doherty, M. F., Design and synthesis of homogeneous azeotropic distillations. 1. Problem formulation for a single column. *Industrial & Engineering Chemistry, Fundamentals* **1985,** 24, (4), 454-463.

66. Taylor, R.; Miller, A.; Lucia, A., Geometry of Separation Boundaries: Systems with Reaction. *Ind. Eng. Chem. Res.* **2006,** 45, (8), 2777-2786.

67. Mulopo, J. L.; Hildebrandt, D.; Glasser, D., Reactive column profile map topology: Continuous distillation column with non-reversible kinetics. *Computers & Chemical Engineering* **2008,** 32, (3), 622-629.

68. Lockett, M. J., *Distillation Tray Fundamentals* Cambridge University Press Cambridge, England, 1986; p 256.

69. Ruiz, G.; Diaz, M.; Sridhar, L. N., Singularities in Reactive Separation Processes. *Ind. Eng. Chem. Res.* **2008,** 47, (8), 2808-2816.

70. Reid, R. C.; Prausnitz, J. M.; Poling, B. E., *The properties of gases and liquids*. McGraw Hill Book Co.,New York, NY: United States, 1987; p Pages: 741.

71. Lee, B. I.; Kesler, M. G., Generalized Thermodynamic Correlation Based on Three-Parameter Corresponding States. *AIChE Journal* **1975,** 21, (3), 510-527.

72. Yaws, C. L., Chemical Properties Handbook In McGraw-Hill: 1999.

73. Kooijman, H. Dynamic Nonequilibrium Column Simulation. Clarkson University, Potsdam, NY, 1995.

74. Ludwig, E. E., *Applied Process Design for Chemical and Petrochemical Plants*. Gulf Publishing Company: 1977; Vol. 2.

75. Colwell, C. J., Clear Liquid Height and Froth Density on Sieve Trays. *Industrial & Engineering Chemistry, Process Design and Development* **1981,** 20, (2), 298-307.